HAWASSA UNIVERSITY

SCHOOL OF POSTGRADUATE STUDIES

COLLEGE OF NATURAL AND COMPUTATIONAL SCIENCE

DEPARTMENT OF CHEMISTRY (SPECIALIZATION; PHYSICAL CHEMISTRY)

GREEN SYNTHESIS OF CO_3O_4/POLYANILINE NANOCOMPOSITES USING *VERNONIA AMYGDALINA* LEAF EXTRACT FOR PHOTOCATALYTIC DEGRADATION OF METHYLENE BLUE AND CONGO RED UNDER SOLAR IRRADIATION

MSc THESIS

BY:

BEZABIH KASAHUN KAYIMO

ADVISORE, Prof. SISAY TADESSE (PhD)

NOVEMBER; 2024

HAWASSA, ETHIOPIA

GREEN SYNTHESIS OF Co_3O_4/POLYANILINE NANOCOMPOSITES USING *VERNONIA AMYGDALINA* LEAF EXTRACT FOR PHOTCATALYTIC DEGRADATION OF METYLENE BLUE AND CONGO RED UNDER SOLAR IRRADIATION

BY

BEZABIH KASAHUN KAYIMO

ADVISOR: prof. SISAY TADESSE (PhD)

A THESIS SUBMITED TO THE DEPARTMENT OF CHEMISTRY, COLLEGE OF NATURAL AND COMPUTATIONAL SCIENCES, SCHOOL OF GRADUATE STUDIES OF THE HAWASSA UNIVERSITY IN PARTIAL FULFILEMENT OF THE REQUIREMENTS FOR THE DEGREE OF MASTERS OF SCIENCE IN PHYSICAL CHEMISTRY

NOVEMBER; 2024

HAWASSA, ETHIOPIA

DECLARATION

I hereby declare that this Thesis entitled **''Green Synthesis of CO_3O_4/Polyaniline Nanocomposites using *Vernonia amygdalina* Leaf Extract for Photocatalytic Degradation of Methylene Blue and Congo Red under Solar Irradiation''** have been my thesis work and has not been presented for a degree in any university.

BEZABIH KASAHUN KAYIMO	_____	_____
Student Name	Signature	Date

This M.Sc Thesis paper has been submitted for examination with my approval as thesis advisor.

Prof. SISAY TADESSE (PhD)	_____	_____
Advisor Name	Signature	Date

ADVISORS' APPROVAL SHEET

SCHOOL OF GRADUATE STUDIES

HAWASSA UNIVERSITY

This is to certify that the thesis entitled ‘‘**Green Synthesis of CO_3O_4/Polyanaline Nanocomposites using *Vernonia amygdalina* leaf Extract for Photocatalytic Degradation of Methylene Blue and Congo Red under Solar Irradiation"** submitted to Department of Chemistry in partial fulfillment of the requirements for the degree of Master of Sciences in Physical Chemistry and has been carried out by **BEZABIH KASAHUN KAYIMO** under my supervision. Therefore I recommended that the student has fulfilled the requirements and hence hereby can submit the thesis paper to the department with my approval as a university advisor.

Prof. Sisay Tadesse (PhD) _____ _____

Advisor Name Signature Date:

EXAMINERS' APPROVAL SHEET

SCHOOL OF GRADUATE STUDIES

HAWASSA UNIVERSITY

We the undersigned, members of the Board of Examiners of the final Thesis open defense by **BEZABIH KASAHUN KAYIMO** have read and evaluated his thesis entitled ''**Green Synthesis of CO_3O_4/Polyanaline Nanocomposites using *Vernonia amygdalina* Leaf Extract for Photocatalytic Degradation of Methylene Blue and Congo Red under Solar Irradiation"** and examined the candidate. This is, therefore, to certify that the thesis has been accepted in partial fulfillment of the requirements for the Degree of Masters of science in Physical Chemistry.

_____	_____	_____
Name of Advisor	Signature	Date
_____	_____	_____
Name of Chairperson	Signature	Date
_____	_____	_____
Name of Internal examiner	Signature	Date
_____	_____	_____
Name of External examiner	Signature	Date
_____	_____	_____
SGS Approval	Signature	Date

Signature Date Final approval and acceptance of the thesis is contingent upon the submission of the final copy of the thesis to the school of graduate studies (SGS) through the Department/ School Graduate Committee (DGC/SGS) of the candidate's department.

Stamp of SGS Date _____

ACKNOWLEDGEMENTS

First of all, I would like to thank Almighty God for his guidance and protections throughout my studies. I sincerely express my deepest gratitude and respect for my advisor Prof. Sisay Tadesse for all of his help, guidance, encouragement and inspiration throughout my research work. I also acknowledge Hawassa University Laboratory technical Mr Tilahun Tumiso for providing a pleasant and friendly working environment in the laboratory during experimental work. I am very grateful to Sidama National Regional State for sponsoring me to do this graduate study and Hawassa University Chemistry Department for accepting me to study my M.Sc. Then I would like to thank Adama Science and Technology University for their support for the characterization of my samples. I am forever grateful to my beloved family, for their unlimited support and initiation through my life, without them this thesis would have not been possible. I also extend my thanks to my friends and classmates who were ultimately participate in this work. Finally, I would like to thank Abera Awaje (MA) for all of his support and advice during this work.

Thanks very much!

Table of Contents

CONTENTS **PAGE**

LIST OF TABLES

LIST OF FIGURES

LIST OF ABBREVIATIONS AND SYMBOLS

CB	Conduction band
CR	Congo red
FT-IR	Fourier transformer infrared
L-H	Langmuir–Hinshelwood
MB	Methylene blue
NCs	Nanocomposites
NPs	Nanoparticles
NMs	Nanomaterials
PANI	Polyaniline
ROSs	Reactive oxygen species
SEM	Scanning Electron Microscopy
TMO	Transition metal oxide
UV-VIS	Ultra violate-visible
VA	*Vernonia amygdalina*
VB	Valence band
XRD	X-ray diffractometer

ABSTRACT

PANI, Co_3O_4 NPs, and Co_3O_4/PANI nanocomposites were successfully synthesized using a green synthesis method and applied for the photocatalytic degradation of Methylene blue (MB) and Congo red (CR). The synthesized materials were characterized using analytical techniques such as XRD, FT-IR, UV-Visible, and SEM. The FT-IR spectra of VA showed that the wavenumber absorption at 3470 cm^{-1} represented the hydroxyl (-OH) group, while at 2931 cm^{-1} characterized the C-H absorption. The peak observed at 1631 and 1402 cm^{-1} indicates C = C stretching and O-H bending of carboxylic acid, respectively. The band at 1173 cm^{-1} corresponds to the C-O stretching of an aromatic ester. The prominent absorption bands at 555 cm^{-1} and 648 cm^{-1}, attributed to the stretching vibrations of the metal-oxygen bond corresponding to (Co^{3+} - O) and (Co^{2+}- O) vibrations, respectively in NPs. A peak at 1628 cm^{-1} and 1401 cm^{-1} shows C=C, and C–N stretching vibration respectively. The characteristic band formed at 3368cm^{-1} corresponding to N–H stretching vibration of secondary amine and for pure PANI, The peak at 1622 cm^{-1} , 1404cm^{-1} is due to the C= C stretching vibration of the quinoid rings ((N=Q=N)) and benzenoid ring (N-B-N) respectively. Band at 1118 cm^{-1} is due to the C−N stretching of a secondary aromatic amine. XRD patterns revealed the crystalline sizes of the materials, with average particle sizes 19.25nm, 8.24nm, 11.03 for Co_3O_4 NPs, PANI powder, and NCs respectively. Morphological investigations indicated unique structures for each material. UV-Visible spectra provided band gap energy values for the synthesized materials (1.69 and 3.93 for Co_3O_4 NPs; 1.57, 3.1 and 4.12 for PANI: 3.26, 3.80 and 5.3 for NCs). The photocatalytic degradation study demonstrated that Co_3O_4 NPs and Co_3O_4/PANI NCs efficiently degraded MB and CR under natural sunlight irradiation. The degradation efficiency was influenced by catalyst dose, initial concentration, pH, and exposure time. Maximum degradation percentages were achieved under optimized conditions for both dyes (93.69% in Co_3O_4/PANI NCS and 90.79% in Co_3O_4 NPs for CR and 91.66% in Co_3O_4/PANI NCs and 89.60% in Co_3O_4 NPs for MB). Co_3O_4/PANI NCs exhibited higher degradation efficiency than Co_3O_4 NPs due to interactions between inorganic semiconductors and conducting polymers. Kinetic studies revealed that MB followed pseudo zero-order kinetics, while CR degradation followed pseudo first-order kinetics with the R^2 = 0.993 and 0.992 respectively.

KEY WORDS: Green synthesis, Co_3O_4, Co_3O_4/PANI, PANI, photocatalytic Degradation, Congo red, methylene blue, *Vernonia amygdalina*.

CHAPTER ONE

1 INTRODUCTION

1.1 Back Ground of the Study

In science and technology, one of the rapidly emerging concepts in the latest year is nanotechnology, which has brought remarkable development. It is a branch of science and engineering that deals with materials having dimensions between 1 and 100 nm. Nanotechnology and science is a multidisciplinary field that exploits the wide spectrum of the emerging area from fundamental sciences such as physics, chemistry, electronics, and material science to develop novel techniques and produce unusual and unique properties of nanomaterial at the Nano scale [1, 2]. Nanotechnology is “the design, characterization, devices, production, and application of structures and systems by controlling shape and size at the nanometer scale” [3].

Nanoparticles are the fundamental components of nanotechnology, with a particle size between 1-100nm and being made from metal, metal oxide, organic matter, and carbon [4]. Nanomaterials are particles that are Nano scale in size, and they are very small particles with improved thermal conductivity, catalytic reactivity, nonlinear optical performance, and chemical stability due to their surface area-to-volume ratio [5]. Nano scale materials have far larger surface areas than similar masses of larger-scale materials. This means that as the surface area per mass of a material increases at the Nano scale, a greater amount of the Nano scale material can come into contact with surrounding materials, thus affecting reactivity and having better catalysts and adsorbents [6].

In recent years, in the field of nanotechnology metal, and metal oxide nanoparticles have been the most developed materials due to their modified and adjustable morphology, physicochemical properties, small size, and enormous surface area [7]. Based on the initial raw materials used, two groups of nanomaterial production processes can be distinguished: top-down and bottom-up approaches. Top-down methods involve the use of mechanical and chemical fabrication processes, and the process of attrition, milling, and etching the bulk material to form nanomaterial (NMs) [8]. Bottom-Up Approaches Compared with top-down methods, bottom-up

methods allow for the creation NMs with fewer faults. In such approaches, atoms, molecules, and nanoparticles are the starting material used to create complex nanostructures [9, 10].

The synthesis of nanoparticles can be done in a variety of ways using physical, chemical, and biological processes. However, the physical and chemical methods require a large amount of chemicals, that until yet leads to poor yield. These are not suitable for the controlled synthesis of nanoparticles rather they are produces toxin substances that pollutant the nanoparticles. Additionally, the majority of chemical methods used to create nanoparticles involve the use of hazardous and toxic chemicals, which pose a risk to human health as well as the environment. [11].

Most important synthesis methods of nanoparticles are through green synthesis approach that is environment friendly, biocompatibility and low toxicity. The advantages of using biological materials such as bacteria, yeasts, molds, microalgae and plant extracts to synthesize NP includes, such as low energy consumption, moderate technology, and no toxic chemicals [12]. In this regard, green synthesis procedures have recently been carried out to produce NPs from biological sources because plant extracts play the role of reservoirs of phytochemicals such as polyphenols, flavonoids, proteins, vitamins, and alkaloids, which act as reducing, stabilizing, and capping agents [13].

Nanoparticles (NPs) are mainly classified into various classes based on their morphology, size, physical & chemical properties. They are mainly classified into organic (composed of organic compounds such as lipids or polymers), inorganic (metal and metal oxides) and carbon based (exist in different shapes such as tube- shaped, horn- shaped, spherical or ellipsoidal.eg fullerene, carbon nanotubes graphene, Nano fibers, and carbon black) NPs. Metal based nanoparticles can be obtained from metals such as aluminum (Al), gold (Au), silver (Ag), cadmium (Cd), cobalt (Co), copper (Cu), iron (Fe), lead (Pb) and zinc (Zn)[14].

Research interest in the synthesis of Nano scale metal oxides is growing due to their quick diffusivities, large surface area, adsorptive qualities, and surface flaws. They exhibit novel material properties that are very different from those of their bulk counterparts due to their small sizes. It has been established that metal and metal oxides nanoparticles are capable of increasing

chemical reaction activities due to the high ratio of surface atoms with free valences to the cluster of total atoms [15].

Cobalt oxide (Co_3O_4) is a remarkable p-type semiconductor with a band gap of 3.95–2.13 eV that comprises a spinel structure with tetrahedral sites occupied by Co^{2+} ions and octahedral sites by Co^{3+} ions, which makes it highly stable and anti-ferromagnetic [16]. Cobalt oxide has drawn increased attention in recent years for the photo degradation of dye pollutants due to its high surface-to-volume ratio, low cost, environment-friendly, easy preparation, and excellent chemical and physical stability. Therefore, Co_3O_4-NPs have vast applications, including lithium-ion batteries, electrochromic devices, magneto-resistive devices, sensors for different organic and inorganic substrates, pigments and dyes, supercapacitors, and selective solar absorbers [17]. Many techniques, including sol-gel, hydrothermal, electrochemical, solvent evaporation, co-precipitation, and green synthesis, are employed in the preparation of the metal oxides. Among these, green synthesis is an inexpensive, eco-friendly, easy process for synthesizing metal oxide nanoparticles. [18].

Research is focused on improvement in effectiveness, efficiency, durability of practical application of nanocomposites by mixing suitable constituents for the synthesis of particular nanocomposites. Nanocomposites are composites in which at least one of the phases shows dimensions in the nanometer range (1 nm $=10^{-9}$m). Transition metal oxide nanoparticles turned out to be widely explored for many applications such as supercapacitors, sensors, solar cell and Photocatalytic applications etc. To improve their efficiency further research have been reported modification of these transition metal oxides mixed/doping with other nanoparticles such as carbon based nanoparticles, metal oxide nanoparticles, conducting polymers etc, it might be useful for new applications in different field of sciences such as chemistry, physics, biology, material science etc. Modification of transition metal oxide based nanoparticles achieve new sets of properties such as enhance surface area, enhanced surface activities, enhanced porosity, decrease in electron hole recombination, increase in conductivities etc [19].

Hybrid composite of polymer and metal oxide nanoparticles have been broadly used as a part of different fields, for example military types of gear, catalysis, safety, defensive suits of clothing, car aviation, and optical gadgets[20]. Among the various conducting polymers, Polyaniline (PANI) has been known to be as a highly effective adsorbent because of its important properties like high surface area, easy preparation, positive surface charge, unique electrochemical performance, environmental stability, and reusability [21].

The presence of certain dyes in water, like MB, malachite green, direct black 38, rhodamine blue, and orange II, can block the passage of light, which can have an adverse effect the development and viability of aquatic plants and algae [22,23]. This, in turn, can disrupt the oxygen levels in the water and endanger aquatic life [14]. One of the dyes that are known to be toxic to aquatic organisms is methylene blue (MB). It Also referred as [7-(dimethylamino) phenothiazin-3-ylidene] dimethylazanium chloride, it is an organic dye with a positive charge that is widely used to color a variety of materials, including leather, paper, clothing, and office supplies [24]. Around 10-15% of the MB generated is usually released into the environment as industrial wastewater. [25]. another organic dye is Congo red which is an anionic diazo dye having color-assisted functional groups. It is commonly used as a coloring material in many industries such as textiles, cosmetics, paper, etc. On the other hand, CR dyes has long been banned owing to its carcinogenic qualities [26].

The presence of dye in wastewater, even at low concentrations, can visibly block sunlight from penetrating the water, causing a reduction in photosynthesis and imposing strict regulations on the organic content of polluted water. Additionally, long term exposure to MB and CR can be detrimental to human health, leading to gastrointestinal issues, central nervous system dysfunction, and kidney damage [27].

Conventional techniques have proven successful in eliminating dyes from waste water; they frequently have drawbacks in terms of cost, efficiency, and selectivity [28]. Nanotechnology reductive degradation has shown significant qualities among the known chemical, physical, and biological approaches for the breakdown of hazardous dyes [29]. Nanomaterials including nanoparticles, nanotubes, and Nano-fibers are used in nanotechnology-based methods to remove colors from water. Due to their large surface area to volume ratio, these materials, which is

enhances their reactivity and makes them more effective in removing dyes from water. They can also be designed to be selective towards specific dyes, which increase their efficiency and specificity [30].

According to recent studies, the compact size and large reactive surface area of transition metal oxides have attracted research interest and paved the way for their use in a variety of areas, including chemical, optical, magnetic, electrical, and catalytic [31,32]. Because of their dual activity, in metal oxide NPs; cobalt oxide (Co_3O_4) NPs and their composites are well suitable to be effective catalysts for water oxidation as well as light absorbers with large band gaps [33, 34]. The plant-mediated synthesis as a green approach is recommended method because it omits the use of harmful chemical reagents. The use of plant extracts also results in surface modification of NPs because of various phytochemicals present in them and conducting polymer composites. Modification of Co_3O_4 NPs achieve new sets of properties such as enhance surface area, enhanced surface activities, enhanced porosity, decrease in electron hole recombination, increase in conductivities and increase photocatalytic degradation of organic pollutants[19].

Vernonia amygdalina is a small tree with brittle branches, up to 10 m tall and commonly called as bitter leaf due to its bitter taste. It is native of tropical Africa but widely found on riverside and lakes areas, in woodland and grassland up to 2800 m altitude, in areas where the average rainfall is 750-2000 mm. The plant is largely utilized in traditional medicine systems and is considered as a therapeutic herb. It is widely grown in Yemen, Ethiopia, South Uganda, Kenya, Tanzania, and Brazil. Its main phytoconstituents are oxalate, phytates, tannins, saponins, flavonoids, cyanogenic glycosides, alkaloids, terpenes, anthraquinone, steroid, coumarins, lignans, xanthones, edotides, sesquiterpenes, and phenol [35]

In this study, an environmentally benign synthesis of Co_3O_4 NPs based composite, i.e. Co_3O_4/PANI composite utilizing the extract of *Vernonia amygdalina* leaf was described and characterization as well as the catalytic degradation application on the CR and MB was evaluated.

1.2 Statement of the Problem

Nature has provided various methods for the synthesis of inorganic materials at the nano and micro scale, leading to a relatively new and largely unexplored area of research focused on biosynthesis of nanomaterials. While chemical and physical methods have been employed for synthesizing Cobalt oxide NPs, these approaches require toxic and expensive chemicals, high temperatures, complex equipment, and produce hazardous by-products that harm the environment. As a result, there is a need for cleaner, sustainable, and environmentally friendly synthesis methods [36].

Thus, to cover this gap, developing easier, safer to use, and plant-mediated synthesis of Co_3O_4/Polyaniline NCs in the green method get the great attention. Due to mutual interactions between inorganic semiconductors and conducting polymers give rise to interesting properties which are significantly different from those of individual components. why because their low thermal conductivity, high electrical conductivity, cost effectiveness, mass production and extensive area processing; Polyaniline, as a conducting polymer, is particularly promising due to its easy synthesis, environmental stability and high electrical conductivity on doping with protonic acids. Therefore, the preparation of PANI composites with Co_3O_4 has gained significant attention due to their distinctive properties and potential applications in various photocatalytic electrical and electronic devices [37].

Synthetic organic dyes discharged from industries causes' substantial environmental pollution as they cannot be degraded by conventional water treatment processes due to their complex aromatic structures, hydrophilic nature, and high stability against environmental factors. Hence, there is a need to develop effective methods to enhance dye degradation, such as NPs and composite catalytic methods. These methods benefit from the high surface area-to-volume ratio of nanoparticles, which increases their reactivity and effectiveness in removing dyes from water. In metal oxide NPs, the cobalt oxide NPs and their composites are well known to be suitable catalysts for water oxidation and as light absorbers with wide band gaps because of their dual activity. The combination of PANI with Co_3O_4 shows improved photocatalytic activity due to the synergistic effects between the two materials. PANI can act as a photosensitizer, enhancing the light absorption of Co_3O_4 and promoting the generation of electron-holes pairs.

Green synthesis method of Co_3O_4/PANI composites is cost-effective and could enable to reduce toxic and reducing chemical constituents because the plant extracts are an effective reducing and stabilizing agent to synthesize metal oxide NPs and have better catalytic efficiency. In this study the extract of *Vernonia amygdalina* was used as a reducing, stabilizing and capping agent for synthesis of Co_3O_4 based PANI composites. Therefore, the combined Co_3O_4/PANI composite has the best photocatalytic degradation performance than individual Co_3O_4 NPs catalysts.

1.3 Objectives of the Study

1.3.1 General objective

The main objective of this study was the green synthesis and characterization of Co_3O_4 NPs and Co_3O_4/PANI NCs using *Vernonia amygdalina* leaf extract and use in Photocatalytic degradation performance of Congo red and methylene blue dyes under solar irradiation.

1.3.2 Specific objectives

- To synthesize PANI, biosynthesis of Co_3O_4 NPs and Co_3O_4/PANI NCs using *Vernonia amygdalina* leaf extract as reducing and capping agent.
- To characterize the PANI, Biosynthesized Co_3O_4 NPs, and Co_3O_4/PANI NCs using XRD, UV-Vis, SEM, and FT–IR instrument.
- To determine the optimum experimental parameters like pH, exposure time, catalyst dose, initial concentration of the dyes and kinetics for the photocatalytic degradation of Congo red and methylene blue.
- To evaluate photocatalytic degradation efficiency of synthesized Co_3O_4 NPs and Co_3O_4/PANI NCs on Congo red and methylene blue dyes.

1.4 Significance of Study

This study will describe a better solution to reduce use of harmful chemical and minimizes waste products by using environmentally friendly green approach to synthesis Co_3O_4 NPs and it's composite. This study will demonstrates the potential for using these synthesized Co_3O_4 NPs and Co_3O_4/PANI NCs in environmental remediation processes, as both Congo red and methylene blue dyes are common organic pollutants in water bodies using solar irradiation as a clean and sustainable energy source for catalysis aligns with the principles of green chemistry. This research will contributes to the development of sustainable nanomaterials and their potential applications in environmental remediation, highlighting the importance of green synthesis in the field of nanotechnology.

CHAPTER TWO

2 LITRETURE RIVIEW

2.1 Nanoparticles

In recent years, considerable attention was given to nanomaterials due to their applications in different fields. The expression “Nanoparticles” called on the particles between (1-100 nm). They show attractive physicochemical properties such as ultra-small sizes (many essential properties are size dependent), high surface area to volume ratios, enhanced mechanical properties, tunable optical emissions, their ability to be active, and concentration i.e., to have to change properties as a function of time or some other variables, and super paramagnetic features. NPs possess very different chemical and physical properties comparative with macro scale particles. Nanoparticles are being used in different fields including electrical, biological textile and chemistry in which shape and size of colloidal metal particles play crucial role in different application including preparation of magnetic, electronic devices, wound healing, anti-microbial gene expression and in the preparation of bio composites [38].

2.2 Classification of Nanoparticles

NPs are mainly classified into organic, inorganic, and carbon based NPs various classes based on their morphology, size, physical & chemical properties.

2.2.1 Carbon based nanoparticles

Carbon-based NPs are nanoparticles which made of carbon. They can take on several forms, including spherical, ellipsoidal, horn-shaped, and tube-shaped. Carbon nanotubes (CNTs) and fullerene are the two main groups of carbon-based NPs. Graphene, carbon black, and nano fibers are other class of carbon-based NPs [14]

2.2.2 Organic nanoparticles

Organic NPs are solid particles with a diameter between 10 nm and 1 μm that are made of organic substances, such as lipids or polymers [39]. Some the well-known organic nanoparticles are ferritin, liposomes, dendrimers, and micelles. They are less expensive, non-toxic, biodegradable, environmentally benign, and suitable in the biomedical field.

Both micelles and liposomes have a hollow core also known as Nano capsules and are sensitive to thermal and electromagnetic radiation.

2.2.3 Inorganic nanoparticles

The particles that are not composed of carbon are known as inorganic nanoparticles [39]. It includes metal and non-metal oxide nanoparticles. As compared with organic NPs in inorganic NPs enormous research and commercial investments has been made.

2.3 Metal Oxide Nanoparticles

Metal oxide NPs are Nano scale particles composed of metal and oxygen atoms. They have a wide range of applications in various fields such as catalysis, electronics, sensors, and medicine due to their unique properties including high surface area, chemical reactivity, magnetic, and optical properties [40]. Due to their remarkably high surface area and superior semiconducting properties, many transition metals and their oxide NPs have been synthesized and tested for photocatalytic performance. Metal oxides such as ZnO, CuO, TiO_2, AgO, and Co_3O_4 are commonly used in photocatalytic dye degradation. Among these Co_3O_4 in particular demonstrated an impressively extensive application for catalysts, sensors, magnetic materials, and energy storage electrode materials [36].

2.4 Synthesis of Metal Oxide Nanoparticles

There are two approaches for synthesizing nanoparticles: "top-down" and "bottom up." The top-down approach the method involves breaking down large-scale bulk material into nano scale particles, which can be achieved by several methods like as milling, attrition process, and electro explosion wire technique. Bottom-up approach Constructing a substance molecule by molecule, atom by atom, and cluster by cluster is known as the bottom method. Physical forces acting on the nanostructure employed to combine the particles into a bigger one during the assembly process [41].

2.4.1 Physical methods of synthesis

The physical methods for NPs synthesis include thermolysis, physical vapor deposition (PVD), pulsed laser method, microwave-assisted synthesis, high energy ball milling, melt mixing, laser ablation, ion implantation, sputter deposition, electric arc deposition, etc. Each of these methods changes one physical parameter; for instance, temperature is changed in thermolysis, pressure in ball milling, pH in ion implantation, laser ablation changes radiation, etc. The desired size and shape of the nanoparticles can be obtained by optimizing and maintaining the optimized parameters. However, primary disadvantages of physical methods include expensive equipment, time-consuming procedures, and higher parameters that are not favorable to the environment [41].

2.4.2 Chemical methods of synthesis

Through chemical reaction processes, the chemical synthesis techniques used to produce metal oxide NPs can be employed to produce more structured and complex nanomaterials. The reducing agent (chemicals) used in these methods are extremely reactive and poisonous substances such sodium borohydride and hydrazine hydrate, which can release hazardous byproducts that can negatively impact the environment, wildlife, and vegetation by releasing toxic by-products [42]. Chemical vapor deposition, solgel, solvothemal process, polymerization, and another chemical precipitation techniques are examples of chemical methods for the synthesis of NPs. most of the chemical methods utilized to synthesize nanoparticles involve the use of hazardous and harmful chemicals, which can create biological risks, and sometimes these chemical processes are not favorable for the ecological environment.

2.4.3 Green methods of synthesis

Green chemistry is the design, development, and implementation of chemical products and processes that reduces or eliminates the use and manufacturing of substances that are harmful to the environment and human health. The green synthesis of Metal NPs and Metal oxide NPs is one of the approaches that utilization biological systems and is based on green chemistry principle. Green synthesis of metallic NPs has been adopted to accommodate various biological materials (e.g., bacteria, fungi, algae, and plant extracts). Using plant extracts is one of the greener ways to manufacture metal/metal oxide nanoparticles that is currently available.

Compared to fungi and/or bacteria-mediated synthesis, this method is very easy and accessible to synthesis NPs at large scale. Green synthesis methodologies based on biological precursors depend on various reaction parameters such as solvent, temperature, pressure, and pH conditions (acidic, basic, or neutral).

Green method is easy, economical, and environment friendly, and has gained a lot of importance in the recently. In green methods plant material such as fruits, leaves, flowers, roots, and seeds extract are used to synthesis metal oxide nanoparticle. For the synthesis of metal/metal oxide nanoparticles, plant biodiversity has been broadly considered due to the availability of effective phytochemicals in various plant extracts, especially in leaves such as ketones, aldehydes, flavones, amides, terpenoids, carboxylic acids, phenols, and ascorbic acids. These components are capable of reducing metal salts into metal nanoparticle [42, 43]. Successful green synthesis of Co_3O_4 NPs has been reported using a variety of plant components, including leaves, stems, roots, seeds, latex, fruits, interior plant parts, peels, and shells. Synthesized eco-friendly Co_3O_4 NPs using the aqueous extract of P. dactylifera L seeds aimed to evaluate the antimicrobial and photocatalytic activity [44]. Punica granatum peel extract was utilized to synthesis Co_3O_4 NPs from cobalt nitrate hexahydrate [45].

In this study, an environmentally benign synthesis of Co_3O_4 NPs based composite, i.e. Co_3O_4/PANI composite was synthesized utilizing the extract of *Vernonia amygdalina* leaf as a reducing, stabilizing and capping agents.

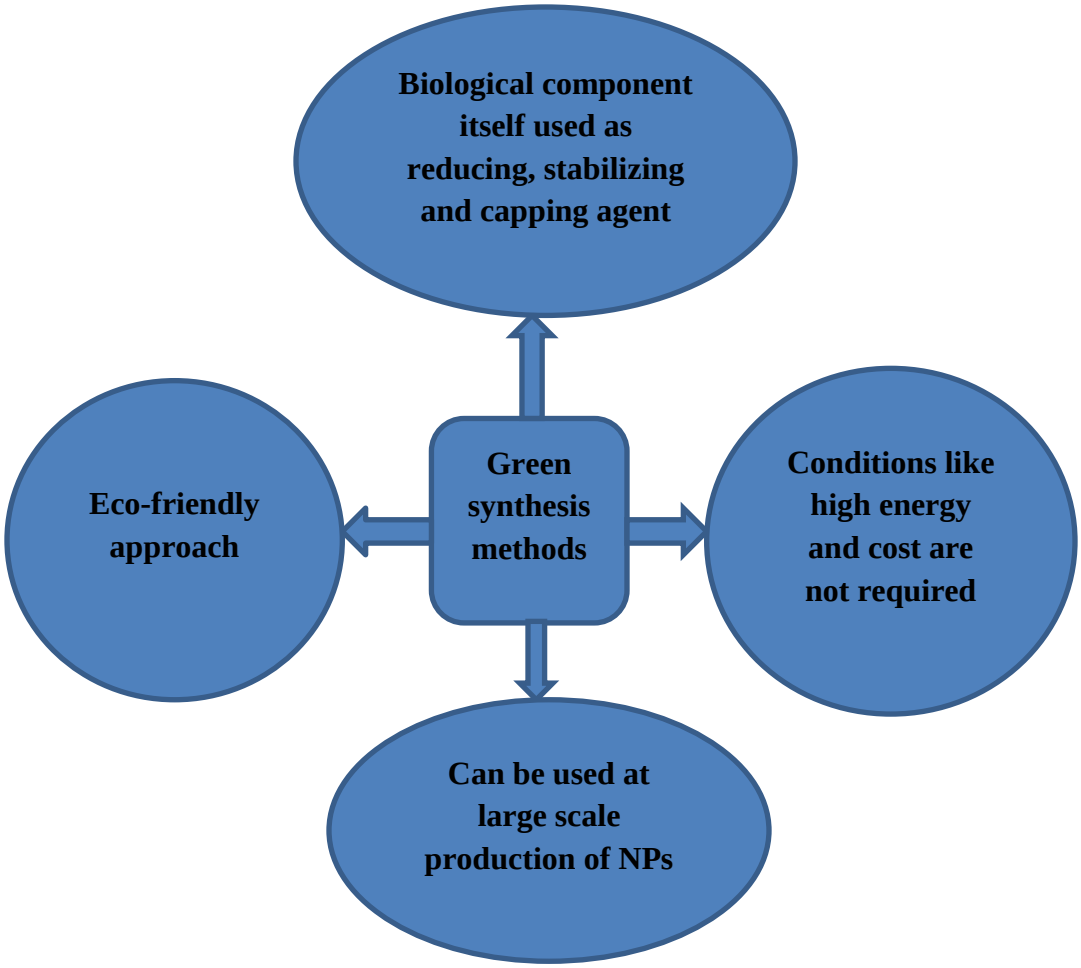

Figure 1: Main benefits of green synthesis method [42]

2.5 *Vernonia amygdalina*

Vernonia amygdalina is a small tree with brittle branches, up to 10 m tall and commonly called as bitter leaf due to its bitter taste. It is native of tropical Africa but widely found on riverside and lakes areas, in woodland and grassland up to 2800 m altitude, in areas where the average rainfall is 750-2000 mm. The leaves are green with a characteristic odor and a bitter taste. The plant is considered as a medicinal herb and mostly used in traditional medicine system. The principal phytoconstituents of the plant are oxalate, phytates, tannins, saponins, flavonoids, cyanogenic glycosides, alkaloids, terpenes, anthraquinone, steroid, coumarins, lignans, xanthones, edotides and sesquiterpenes and phenol. The plant attributed with anti-cancer, ant diabetic, anti-malarial, anti-inflammatory, cathartic, hepatoprotective, antimicrobial, and antioxidant. The species is

widely cultivated in Yemen and Ethiopia, South Uganda, Kenya and Tanzania, Brazil. VA (Tribe Veronica of family Asteraceae) is a shrub or small tree of 2-5 m. It grows well under full sunlight in humid conditions as well as fairly well in drought conditions. It can be found on all soil types, but performs best in humus-rich soils. In cultivation it is mostly pruned to a shrub or hedge. Plant grows in wide ecological zones in Africa and produces large mass of forage used for medicinal and vegetable use [35].

2.6 Plant Extract Role in TMOs Based Nanoparticle Synthesis

An extensive biological source from plant extracts and microrganisms help to synthesis nanoparticles from their metal precursors. Preparations of efficient TMOs nanocatalyst with chemical wet methods are highly affect the environment safety due to the corrosive nature of chemicals which were used as a reducing agent during synthesis. Therefore, finding safe, simple, green, and alternative to the wet chemical method are highly encouraged to keep the safety of lives found on the ecosystem. Therefore, preferring a plant lead nanoparticle synthesis method is chosen as a green and time saving approach [36].

Phytochemicals that extracted from leaves, flowers, roots, stems, and seeds have a reducing and stabilizing agent activity as reported from many research works. Their primary reductant activity nature they enhance nanoparticle reducing capability from their metal precursors of plant extracts, various metal oxides nanoparticles have been well prepared. In addition to their stabilizing ability, extracts have also a role to prevent nanoparticles from surface aggregations which is commonly known as capping agent. The presence of dense aggregation reduces the reactive sites of the active nanoparticles which then reduce the active surface area. It is reported that, plants contain various kinds' phytochemicals from terpenoids, organic acids, and many others. It has been elucidated that those organic compounds contains an active functional groups, such as hydroxyl, aldehyde, amine, and carboxyl units, which are a primary source of electrons and could increase the reduction and stabilization of nanomaterials [13,53].

In this study *Vernonia amygdalina plant* leaf extract was used as stabilizing and reducing agent in green synthesis of cobalt oxide nanoparticle. It is native of tropical Africa but widely found on riverside and lakes areas, in woodland and grassland up to 2800 m altitude, in areas where the

average rainfall is 750-2000 mm and it is a member of the Asteraceae family. Leaves are green with a characteristic odor and a bitter taste .The plant is considered as a medicinal herb and mostly used in traditional medicine system.

2.7 Cobalt Oxide (Co_3O_4) Nanoparticles

Transitional metal oxides are an important class of materials, due to their attractive magnetic, electronic, and optical properties. This makes them effective for use in a variety of applications, such as catalysis, sensor, and lithium ion batteries for energy storage applications [46]. Among these, Co_3O_4 in particular demonstrated an impressively extensive application and has attracted numerous research interests due to its low cost and good electroactivity. Cobalt oxide (Co_3O_4) nanoparticles are transition metal oxide NPs with variable oxidation states that are used in a variety of applications such as gas sensors, pigments, catalysts, magnetic materials, electronic devices, anode materials for rechargeable batteries, high-temperature solar selective absorbers and solar energy system magnetic devices and biological applications, such as antibacterial, anticancer, antioxidant, antifungal, and enzyme inhibition properties. Co_3O_4 NPs have a conventional cubic spinel crystal structure, in the oxidation state of Co (II) occupying tetrahedral sites and octahedral sites in the Co (III) oxidation state. Co_3O_4 is a known multifunctional, antiferromagnetic p-type semiconductor with spinel crystal structure. The direct optical band gaps of Co_3O_4 NPs is about 1.48 and 2.19 eV and it can be used as photocatalyst to degrade several organic pollutants using visible light [47-49].

Combinations of biocompatible redox polymers with low-cost inorganic NPs as a composite have attracted considerable attention in many areas of research. Modification of transition metal oxide based nanoparticles achieve new sets of properties such as enhance surface area, enhanced surface activities, enhanced porosity, decrease in electron hole recombination, increase in conductivities etc. So, researchers usually combined different TMO with conducting polymers to modify conventional material properties such as electrical conductivity, compatibility, and dispersibility [50]. Therefore the combination of PANI with Co_3O_4 shows improved photocatalytic activity due to the synergistic effects between the two materials. PANI can act as a photosensitizer, enhancing the light absorption of Co_3O_4 and promoting the generation of electron-hole pairs.

2.8 Conducting Polymer (PANI)

Conducting polymers play a crucial role in the field of nanoparticles due to their unique electrical, optical, and mechanical properties. These polymers have been widely used as coatings, templates, and stabilizers for nanoparticles, allowing for the development of novel materials with enhanced functionalities. The conducting polymer coating not only provided excellent stability and dispersibility to the nanoparticles but also improved the electron transfer kinetics, leading to enhanced sensitivity and selectivity in the detection of target analytes [51]. Conducting polymers such as Polyaniline, polythiophene, polyacetylene, and polyethylene have been synthesized as organic–inorganic hybrid nanocomposite materials and because of their inimitable potentials and unique electrical, optoelectronic and chemical properties attributed to the presence of extended π-conjugated electron system along the backbone of the conjugated materials they are used in many scientific researches related to sensors, batteries, electronics, electromagnetism, electroluminescence, thermoelectricity, and electro mechanics. Among the several conducting polymers, Polyaniline (PANI) has been known to be as a highly effective adsorbent because of its important properties like high surface area, easy preparation, positive surface charge, distinctive electrochemical performance, environmental stability, and reusability [21].

2.9 Co_3O_4/PANI Nanocomposites

Nanocomposites are composites in which at least one of the phases shows dimensions in the nanometer range (1 nm =10^{-9}m). Conducting polymer composites is some suitable composition of a conducting polymer with one or more inorganic nanoparticles so that their desirable properties are combined successfully. Inorganic–organic composite materials are important due to their extraordinary properties, which arise from the synergism between the properties of the components. These materials have gained much interest due to the remarkable change in properties such as mechanical, thermal, electrical, and magnetic compared to pure organic polymers [52]. Metal oxide-Polyaniline (PANI) nanocomposites have attracted significant attention due to their unique electrical, optical, and catalytic properties. These nanocomposites are promising materials for various applications such as sensors, energy storage devices, and environmental remediation. Among them Co_3O_4/PANI nanocomposite has gained significant attention in recent years due to its unique properties and potential applications in various fields

such as energy storage, catalysis, and sensors. This nanocomposite combines the high conductivity of Polyaniline (PANI) with the high capacity and stability of Co_3O_4, making it an attractive material for advanced technological applications [53].

2.10 Organic Dyes and Its Toxicity

Dyes are colored organic compounds that are used to color various substances like fabrics, paper, food, hair and drugs etc. Dyes may be defined as substance that when applied to a substrate provides color by a process that alters, at least temporarily, any crystal structure of the colored substances. Industry play major role in the providing human need and improving their life style however the negative consequence of industrial activities such as paper, printing, textile, and pharmaceutical manufacturing due to existence hazardous chemical and dyes in their effluents cannot be ignored. The world now is use large amount of dyes in the Textile, leather, food, agro industries for colored their productions. Especially these dyes are chemical aromatic compounds have very complex structures which become a serious environmental problem, such as the color is aesthetically objectionable. Conventional methods have been effective in removing dyes from water, but they often have limitations in terms of efficiency, selectivity, and cost [28].

Among the existing chemical, physical, and biological methods for the degradation of harmful dyes, nanotechnology reductive degradation has demonstrated significant qualities [29]. Nanotechnology-based approaches for the degradation of dyes from water include the use of nanomaterials such as nanoparticles, nanotubes, and nanofibers. These materials offer a high surface area-to volume ratio, which enhances their reactivity and makes them more effective in removing dyes from water. They can also be designed to be selective towards specific dyes, which increase their efficiency and specificity.

Table 1: Classification of dyes

Dyes	Description
Acidic	Water-soluble anionic compound
Basic	Water-soluble, applied in weakly acidic dye baths; very bright dyes
Direct	Water-soluble, anionic compounds; can be applied directly to cellulosic without mordents (or metals like chromium and copper)
Disperse	Not water-soluble
Sulfur	Organic compounds containing sulfur or sodium sulfide
Vat	Water-insoluble; oldest dyes; more chemically complex

2.10.1 Congo red

Congo red is an azo group of dyes which is acidic (anionic) in nature. Congo red has been extensively used in textile industry and it has number of harmful effects on environment and human. It is carcinogenic and causes irritation in human respiratory system. Congo red is a heterocyclic aromatic chemical compound with molecular formula, $C_{32}H_{22}N_6Na_2O_6S_2$. It gives red colored solution in aqueous phase at PH>5 and the color changes to blue at more acidic PH. The molecular weight of Congo red dye is 696.663219, λmax = 510 nm [54]. Its molecular structure in 2 dimensions shown as follows

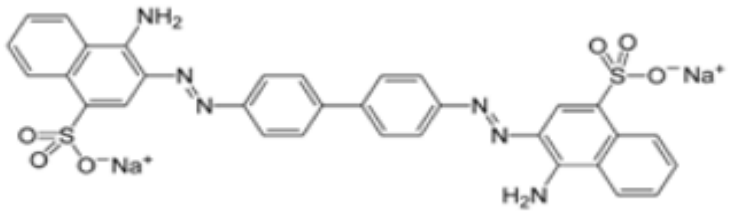

Figure 2: Chemical structure of Congo red

2.10.2 Methylene Blue

Methylene Blue (methylthionine chloride) is a heterocyclic aromatic chemical compound with molecular formula $C_{16}H_{18}ClN_3S$. It is a cationic thiazine dye that is deep blue in the oxidized state while colorless in its reduced form leucomethylene blue. Various types of dyes, including methylene blue used in dye, paint production and wool dying [55]. MB also used as a sensitizer in photo oxidation of organic pollutants.

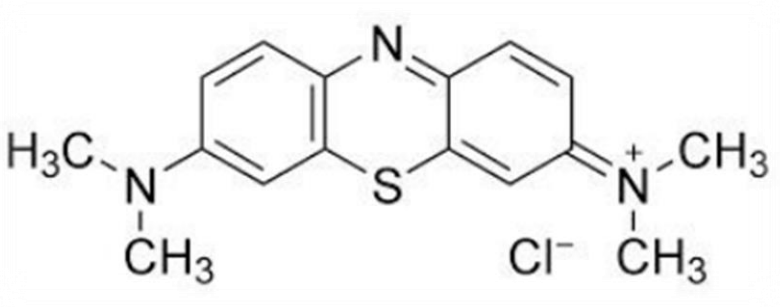

Figure 3: Molecular structure scheme of methylene blue

Table 2: physical and chemical property of Methylene blue dye

Physical and chemical properties	Values
Melting point	180℃
Solubility in water	35.5g/l
pH value	3
Molecular weight	319
Color	Dark blue-green in oxidized form, colorless in reduced form
Chemical formula	$C_{16}H_{18}ClN_3S$

2.11 Photocatalysis

Photocatalysis is defined as a photo induced reaction which is accelerated by the presence of catalysts. These reactions activated by the absorption of a photon with the sufficient energy (equal or higher than the band-gap energy) of the catalysts [56]. The term photocatalyst is a

combination of two words: photo related to photon and catalyst, which is a substance altering the reaction rate in its presence. Therefore, they are materials that change the rate of a chemical reaction on exposure to light. Photocatalysis includes reactions that take place by utilizing light and a semiconductor. The substrate that absorbs light and acts as a catalyst for chemical reactions is known as a photocatalyst. All the photocatalysts are basically semiconductors.

Photocatalysis is a phenomenon, in which an electron-hole pair is generated on exposure of a semiconducting material to light. Absorption leads to a charge separation due to promotion of an electron from valence band of the semiconductor to the conduction band, thus generating a hole (h^+) in the valence band. The recombination of the electron and the hole must be prevented as much possible if a photocatalzed reaction must be favored. The ultimate goal of the process is to have a reaction between activated electrons with an oxidant to produce a reduced product, and also a reaction between the generated holes with a reductant to produce an oxidized product. The photo generated electrons could reduce the dye or react with electron accepters such as O_2 adsorbed on semiconductor surface or dissolved in water reducing it to superoxide radical an ion $O_2^{\cdot-}$.

The photocatalytic reactions can be categorized into two types on the basis of appearance of the physical state of reactants. Homogeneous photocatalysis: When both the semiconductor and reactant are in the same phase, i.e. gas, solid, or liquid, such photocatalytic reactions are termed as homogeneous photocatalysis. Heterogeneous photocatalysis: When both the semiconductor and reactant are in different phases, such photocatalytic reactions are classified as heterogeneous photocatalysis [57].

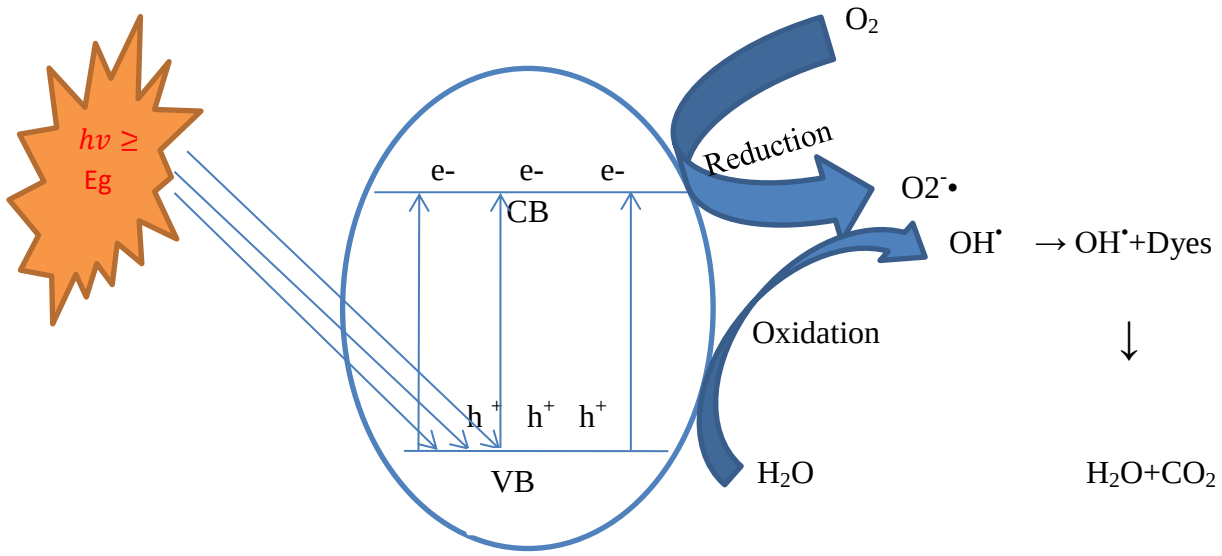

Figure 4: Representations of the photocatalysis in a semiconductor material [58, 59].

2.12 Photocatalytic Degradation of Dyes

Photocatalytic degradation of dyes is a process that uses photocatalysts to break down and remove dyes from water or other solutions. This method involves the use of a catalyst, semiconductor, such as titanium dioxide, zinc oxide and etc, which becomes activated when exposed to light. When the photocatalyst is activated by light, it generates reactive oxygen species that can oxidize and break down the dye molecules into smaller, less harmful compounds. This process is often used in wastewater treatment plants to remove dyes from industrial effluents before they are released into the environment. It is also being studied for potential use in the treatment of contaminated groundwater and other water sources.

The advantages of photocatalytic degradation of dyes include its effectiveness in breaking down a wide range of dye molecules, its ability to operate under ambient conditions, and its potential for use in continuous flow systems [60]. The photocatalytic degradation process of Co_3O_4 NPs involves the use of light energy to initiate a chemical reaction that breaks down organic compounds into smaller, harmless molecules. This is associated with the breakdown of the chromophoric group and the transformation of dye into low-molecular-weight by-products. The dye degradation is mainly due to generating electrons and holes (e^- & h^+) on the catalyst surface under irradiation. Under visible light, Co_3O_4 NPs undergo charge separation, and electrons in the valence band of Co_3O_4 can be excited to its conduction band ($e^-_{C.B}$), causing the generation of

holes in the valance band ($h^{+}_{V.B.)}$ simultaneously (Equation (1)). Thus, the OH· generated from the reaction (Equation (2)) is the main factor for the photo degradation of the dye because it is a strong oxidizing species, known to be an oxidation process. These ROSs can then react with organic molecules, such as pollutants or contaminants, breaking them down into smaller, less harmful compounds such as carbon dioxide and water [36].

$$Co_3O_4 + hv \rightarrow e^{-}_{CB} + h^{+}_{VB} \quad (1)$$

$$H_2O + h^{+}_{VB} \rightarrow H^{+} + OH^{\bullet} \quad (2)$$

$$Co_3O_4\,(e^{-}) + O_2 \rightarrow {}^{\bullet}O_2^{-} + Co_3O_4 \quad (3)$$

$$\text{Dyes} + OH^{\bullet} / {}^{\bullet}O_2^{-} \rightarrow \text{Degradation products } (CO_2, H_2O) \quad (4)$$

2.13 Experimental Parameters for Photocatalytic Degradation

Several studies have been reported the significance of operational parameters. The photo degradation depends on the some basic parameters which are initial concentration of dyes, amount of photocatalyst, pH of the solution, temperature of reaction medium, the intensity of light, nature of the substrate, dopant. The oxidation rates and efficiency of the photocatalytic system are highly dependent on a number of operational parameters that govern the photo degradation of the organic molecule [61].

2.13.1 Effect of initial concentration of dye

The photocatalysis is depends on the adsorption of dyes on the surface of photocatalyst. In the photocatalysis process, only the amount of dye adsorbed on the surface of photocatalyst contributes and not the one in the bulk of the solution. The adsorption of dye depends on the initial concentration of dye, as the initial dye concentration increased, several monolayer of adsorbed dye formed, resulting in more adsorbed molecules available for the degradation. Until reaching critical level, constant rate is obtained because the surface is completely covered the degradation rate is however, decreased with the further increase [62].

2.13.2 Effect of pH

The Photo degradation of dyes is affected by the pH of the solution. The variation of solution pH changes the surface charge of semiconductor particles and shifts the potentials of catalytic reactions. As a result, the adsorption of dye on the surface is altered thereby causing a change in the reaction rate. The pH determines the surface charge of the photocatalyst. Adsorption of the dye is minimum when the pH of the solution is at the isoelectric point (point of zero charge). The surface of the photocatalyst is positively charged below isoelectric point and carries a negative charge above it [63].

2.13.3 Effect of photocatalyst load

Degradation of dye is affected by the amount of the photocatalyst. The photo degradation of dye increases with increasing catalyst amount, which is the feature of heterogeneous photocatalysis. The increase in catalyst amount actually increases the number of active sites on the photocatalyst surface thus causing an increase in the formation of number of •OH radicals which can take part in actual discoloration of dye solution. Beyond a certain limit of catalyst amount, the solution becomes turbid and thus blocks UV radiation for the reaction to proceed and therefore percentage degradation starts decreasing [64].

2.13.4 Effect of light intensity

The intensity of light affects photo degradation and it determines the extent of light absorption by the semiconductor catalyst at a given wavelength. The degradation efficiency of dyes using a semiconductor photocatalyst depends on the intensity of light [65]. An increase in the intensity of light will result in increased photocatalytic reaction rates.

2.14 Kinetics Study of Photocatalytic Degradation Reaction

Photocatalytic oxidation reaction of organic compounds is a surface reaction, and the rate equation often expressed by the Langmuir-Hinshelwood (L-H) model as follows [66]

$$\boldsymbol{r = -\frac{dc}{dt} = \frac{kKC}{1+KC}} \qquad (5)$$

In which C is the concentration of reactants; t is reaction time; k is the rate constant, K is the adsorption constant. The kinetic parameter of k and K are affected by light intensity, temperature, the initial concentration and physical properties of reactants and etc.

In order to determine the degradation rate of organic compounds under optimal conditions, kinetic studies can be conducted by applying a pseudo–zero, pseudo-first-order and second-order reaction rate [67].

$$\boldsymbol{Co - Ct} = k_O t \quad (6)$$

Pseudo-zero-order reaction rate Equation

$$\mathbf{ln}\left(\frac{\boldsymbol{Co}}{\boldsymbol{Ct}}\right) = k_1 t \quad (7)$$

Pseudo-first-order reaction rate

$$\frac{\mathbf{1}}{\mathbf{Ct}} - \frac{\mathbf{1}}{\boldsymbol{Co}} = k_2 t \quad (8)$$

Pseudo-second-order reaction rate

Where t (hr) is the reaction time, C_0 is the initial concentration, Ct is the concentration at time t, k_1 (hr^{-1}) and k_2 (L/mghr) represents the first-order and second-order reaction rate constant. The rate constant (k) of first-order reaction will be obtained by plotting ln (C_0/Ct) against the reaction time t and 1/Ct- 1/Co against time (t) for second-order reaction.

CHAPTER THREE

3 MATERIALS AND METHODS

3.1 Chemicals and Reagents

Cobalt nitrate hexa-hydrate [$Co(NO_3)_2.6H_2O$; purity 99.9%] as metal oxide precursor, Ammonium persulphate [$(NH_4)_2S_2O_8$ 98% , Sigma- Aldrich], aniline ($C_6H_5NH_2$ 99.5%, Merck), sodium hydroxide (NaOH) Sigma Aldrich, hydrochloric acid HCL (37%, Merck) fresh and healthy *Vernonia amygdalina* leaf, distilled water along with the leaf extracts were used for synthesis of nanoparticle, Congo red (anionic) and methylene blue (cationic) dyes from Hawassa university main campus chemistry laboratory room was taken and used as organic pollutant to study photocatalytic degradation.

3.2 Apparatus and Equipment's

Grinding machine (s-707, HALNDEN WANGER, BERLIN) was used for grounding; Oven (INSIF, India Ho 13301) used for drying purpose. Electronic balance (Sartorius AG, Germany) was used for measure extract powder and precursor salts. Muffle furnace (INSIF, India, Ho) was used for calcination the prepared Co_3O_4 NPs, PANI and Co_3O_4/PANI nanocomposites, beaker (SCHOTT DURAN, Germany), pH meter (CG 841, Germany), Refrigerator (SM-480, Germany), measuring cylinder (Superte, Borosilicate glass), Whatman filter paper (made in India), magnetic stirrer hot plate (INSIF, H-359), centrifuge (Labofuge 200, Germany), glass filters, test tube (EIS, Pyrex glass), and round bottom flask (Bo MEX), were used for multipurpose.

X-ray diffractometer (XRD- 7000, Shimadzu Corporation, Japan model), Scanning electron microscopy (SEM) (JEOL - JSM-IT300L), UV-Vis Diffuse reflectance spectroscopy (JASCO V-670 UV – VIS), and Fourier transforms infrared (FT-IR) spectra Perkin Elmer FT-IR BX spectrophotometer were used to characterize PANI, greenly synthesized Co_3O_4 NPs, and Co_3O_4/PANI composites.

3.3 Plant Sample Collection Site

A fresh and healthy leaf of *Vernonia amygdalina* was collected from Wotiko Bona Zuria woreda, Sidama regional state, Ethiopia which is 284 km from Addis Ababa and 104 Km from Hawassa.

3.4 Preparation of *Vernonia amygdalina* Extract

Vernonia amygdalina leaf extract was prepared according to literature obtained from [68] with little modification as follows. Briefly VA leaves was collected and washed with distilled water and dried at room temperature for four days (96h). Then the dried VA leaves was grinded in Electric grinder to obtain fine powder. After that 10 g of powder of VA was mixed with 100 ml of Distilled water in Erlenmeyer flask and heated at 80 °C while stirring using magnetic stirrer for 1 h. finally the heated VA solution was allowed to cool for 3 h and then filtered by using Whatman no 1 filter paper to obtain a fine *Vernonia amygdalina* extract solution and was stored in refrigerator for the further experiments. The schematic diagram for preparation was shown in Figure 5 as follow

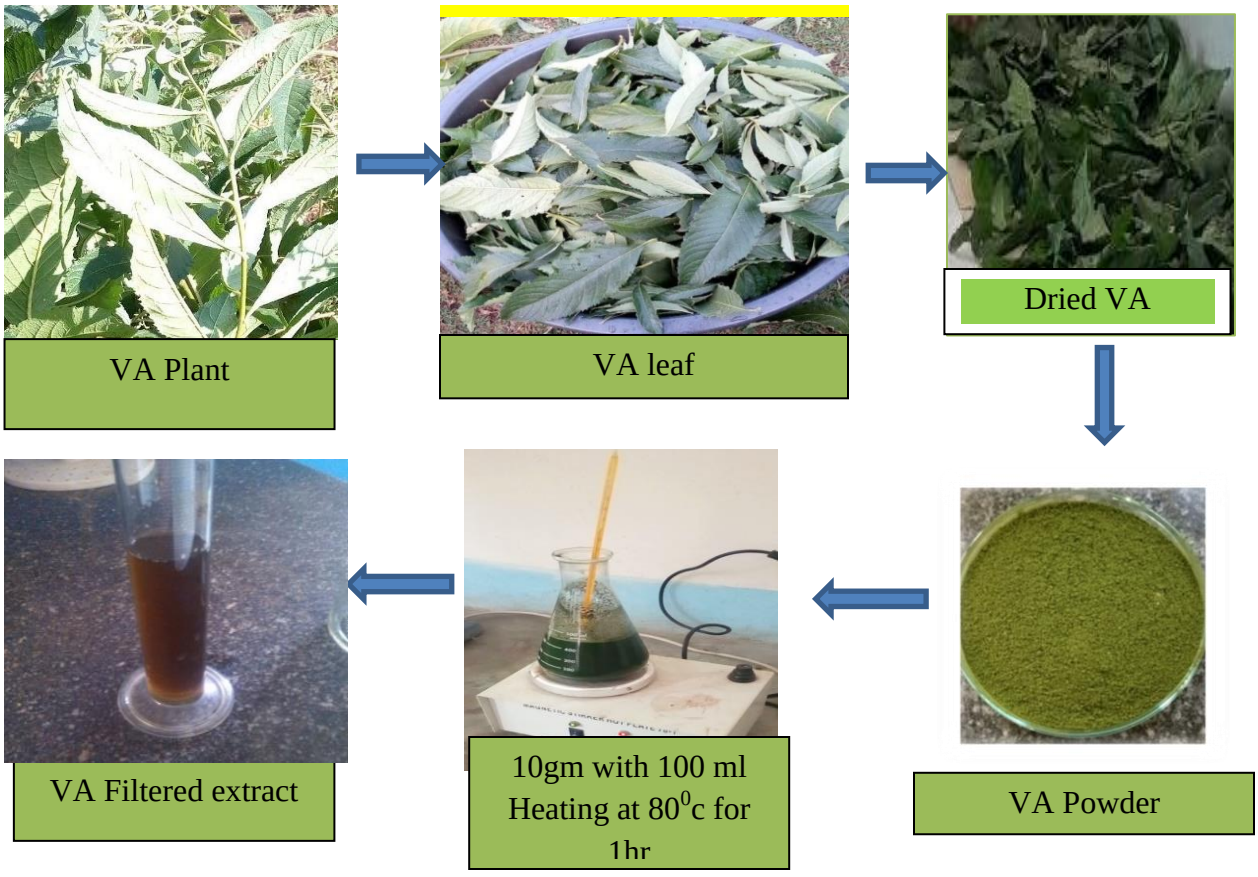

Figure 5: Flow chart for the preparation of pure *Vernonia amygdalina* leaf extract

3.5 Green Synthesis of Co_3O_4 Nanoparticles

Co_3O_4 NPs was synthesized using the green synthesis method, which used *vernonia amygdalina* aqueous extract as a reducing agent with the little modification of [69]**.** Accordingly, 0.2 M solution of Co $(NO_3)_2 \cdot 6H_2O$ was prepared, next 120ml placed in 500ml beaker and mixed with 30 ml of *VA* leaf extract through continuously stirring in a beaker and 0.1 M sodium hydroxide solution was added to adjust pH until it reached 10, rsulting deep green color appearance**.** The mixture was stirred using a magnetic stirrer at 85^0C untill the the color changed from deep green to blak. Finally the mixture was collected, calcined in muffle furnace at 400 °C for 2h, grinded and stored for further experimental use.

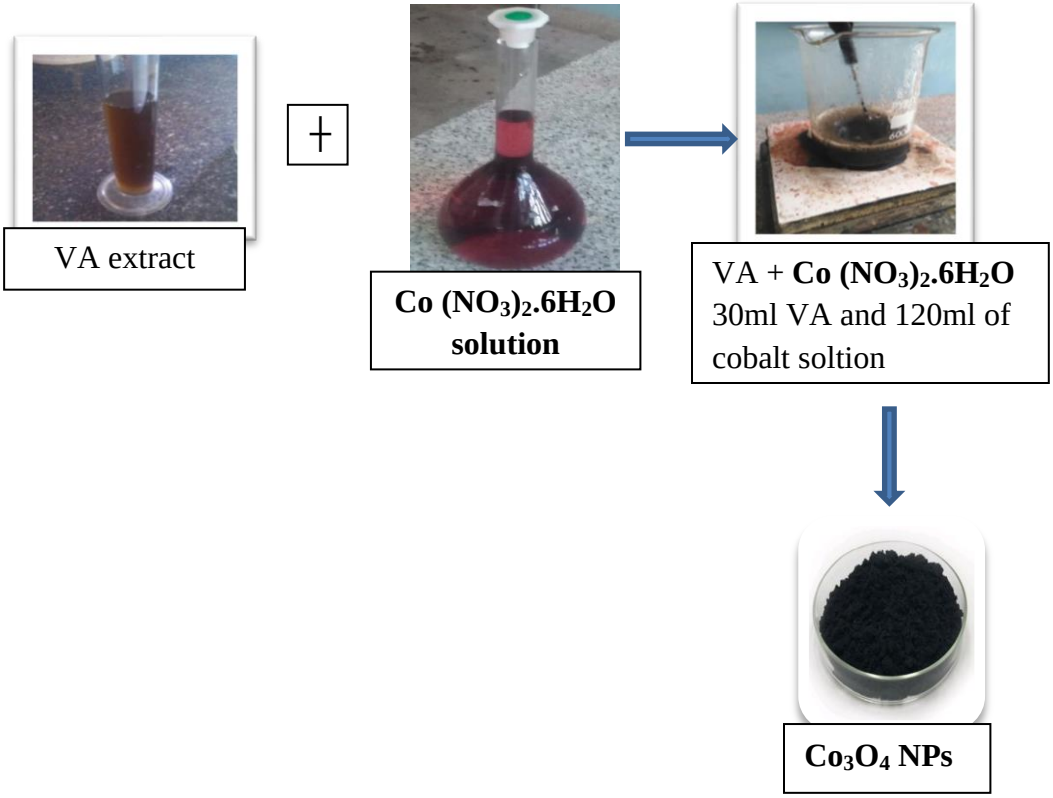

Figure 6: Flow diagram for green Synthesis of the Co_3O_4 Nanoparticles

3.6 Synthesis of PANI

Synthesis of PANI was based on mixing aqueous solution of aniline hydrochloride and ammonium persulphate (APS) at room temperature, followed by the separation of PANI Hydrochloride precipitate by filtration and drying adopted from the literature [70]. Briefly, 0.5 ml aniline monomer was dissolved in 1 M (100 ml) HCl aqueous solution in a Beaker and stirred for 30 minute accordingly. Next, 5.71 g of ammonium per sulfate (APS) was dissolved in 50 ml of distilled water. Both solutions were kept each separately for 1 h at room temperature. Then, the two solutions were mixed in a beaker and stirred with a magnetic stirring bar until the color change from colorless to dark green, which was indicated PANI formation, and was wait for 4 hrs to polymerize. The formed PANI precipitate was collected by filtration and wash with 0.2 M HCl solution until the filtrate becomes clear, then with ethanol several times to remove monomer, oligomer as well as with distilled water several times to remove the acid. Finally, PANI powder was dried in an oven at 60°C for 24 h.

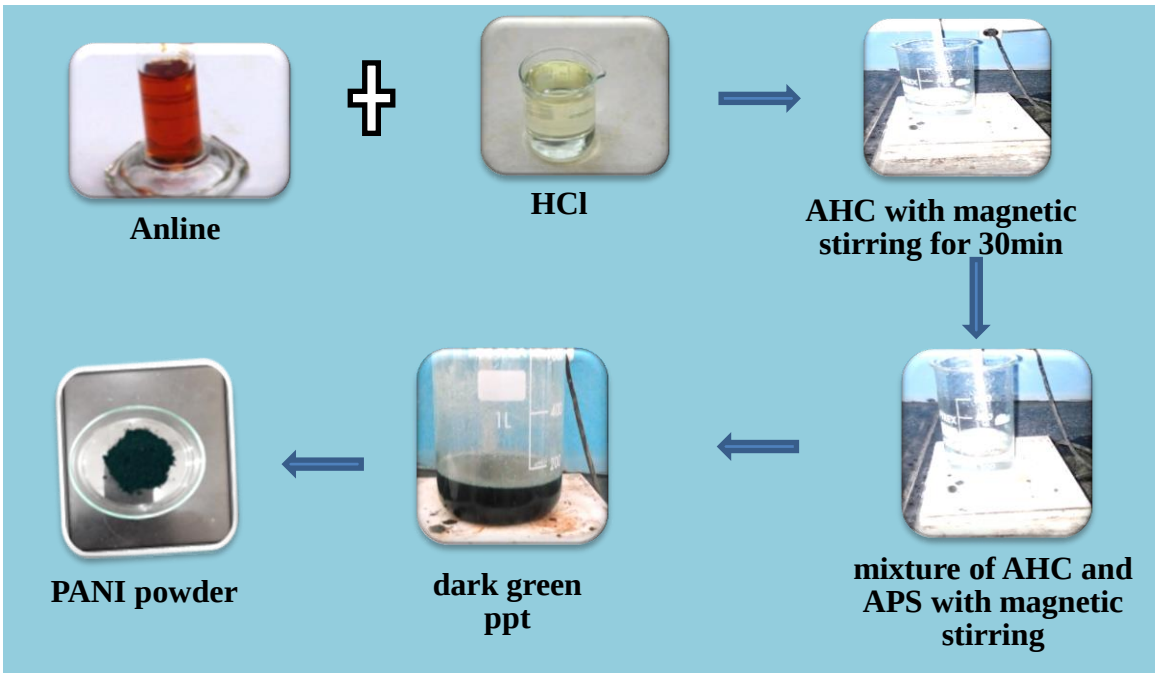

Figure 7: Flow chart for the preparation of polyaniline (PANI)

3.7 Synthesis of Co_3O_4/PANI nanocomposites

A typical in situ oxidative polymerization method was used to synthesis Co_3O_4–based PANI Nanocomposites by following [71] with little modification. Firstly (protonation step), 0.5 ml aniline (0.1 M) monomer was adedd in 1 M HCl (100 ml) aqueous solution in a beaker and stirred for 30 min to form aniline hydrochloride. Secondly (homogenization of oxidant), 0.5 g of green synthesized Co_3O_4 NPs was dissolved in 25 ml distilled water for 5 min in order to keep the Co_3O_4 homogeneously suspended in the solution. Finally, a homogeneously suspended Co_3O_4 NPs was added drop wise to doped aniline hydrochloride solution with 2.86 g APS (co-dopant) at room temperature, and the mixture was stirred continuously at room temperature for 4 h to complete the polymerization process. The reaction mixture was turned into dark green precipitate, the obtained materials was then collected by filtration and washed with 0.2 M HCl solution until the filtrate become clear, then with ethanol several times to remove monomer, oligomer as well as with distilled water several times to remove the acid. Finally, the product was dried in the oven at 60°C for 24h to obtaine dried Co_3O_4/PANI nanocomposites.

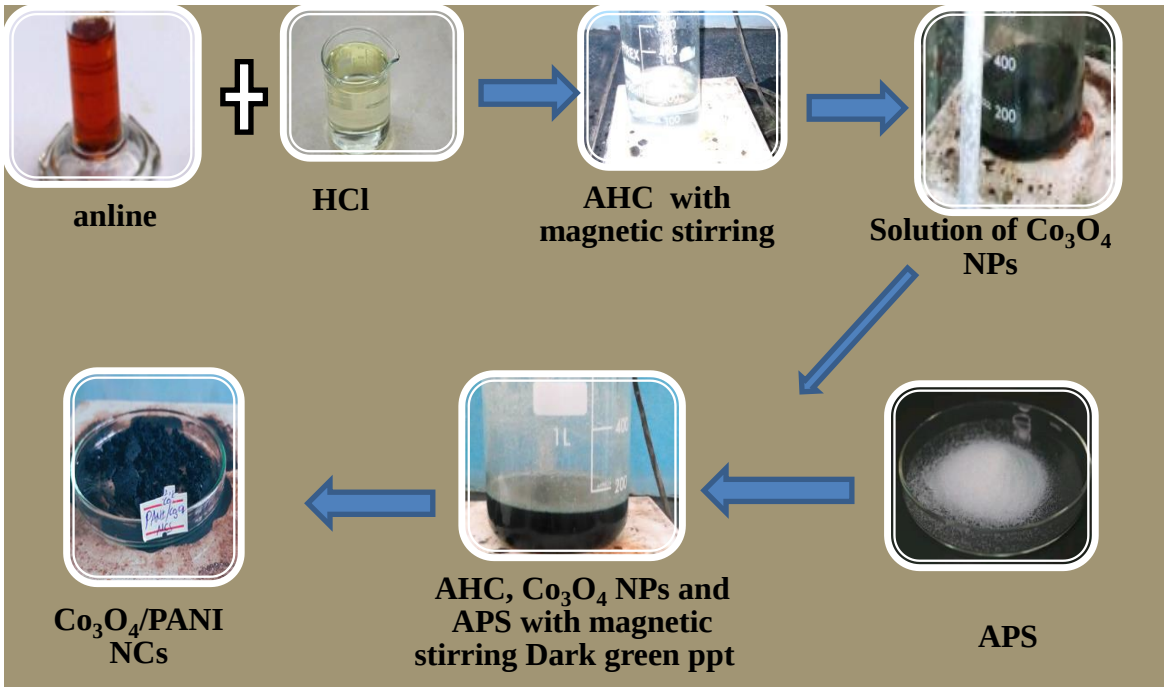

Figure 8: Flow chart for the preparation of Co_3O_4/PANI nanocomposites

3.8 Characterization Study

3.8.1 Uv-visible Spectrophotometry analysis

Optical properties of the synthesized PANI, Co_3O_4 NPs, and PANI/Co_3O_4 nanocomposite were confirmed by double beam Uv–visible spectroscopy (Azzota S M-1600 SPECTROPHO-TOMETER , USA) in the range of 200-800nm.

3.8.2 Scanning Electron Microscopic (SEM) analysis

The surface roughness, pore structure, and pore size distributions of synthesized Co_3O_4, PANI, and Co_3O_4 /PANI nanocomposite surfaces was studied by using a Scanning electron microscopy (SEM) (JEOL - JSM-IT300L).

3.8.3 X-ray Diffraction (XRD) analysis

The crystalline structure of synthesized PANI, Co_3O_4 NPs, and PANI/Co_3O_4 nanocomposite was performed using Shimadizu X-ray diffractometer (XRD- 7000, Shimadzu Corporation, Japan model) with a voltage of 40kv and a current of 30mA using at(cu kα=1.50406Å) radiation as X-ray source in the 2θ range from 10° to 80°. From the XRD data obtained, the crystalline size of sample was calculated using Debye-Scherer's formula a shown below:-

$$D = \frac{k\lambda}{\beta COS\theta} \qquad (9)$$

Where D is average crystalline size, k is Scherer constant (usually 0.9), λ is wave length of X-ray source Cu kα radiation (1.5406 Å), β is full width at half- maximum (FWHM) of the diffraction in radian.

3.8.4 Fourier Transform Infrared (FT- IR) spectra analysis

The intermolecular bonding vibration and stretching motion of the all samples was performed by Fourier transform infrared (FTIR Perkin Elmer65, Perkin Elmer, Inc., Waltham USA) in the range of 4000-400cm^{-1} with samples prepared using KBr pellets.

3.9 Photocatalytic Activity Study of Co_3O_4 NPs and Co_3O_4/Polyaniline NCs

The photocatalytic activity of biosynthesized Co_3O_4 NPs and PANI/Co_3O_4 nanocomposite were evaluated using Congo red and methylene blue dyes with little modification [72]. The solar light source irradiated the Co_3O_4 NPs and composite. To evaluate effectiveness of the synthesized NPs and NCs, optimized amount was added in to the beaker containing 25ml of prepared MB and CR aqueous solution separately in a dark environment. The dark condition stirring process helps to attain the adsorption-desorption equilibrium positions Visible light photocatalytic activity was processed under solar irradiation .The light irradiation dissociated the dye bonding and decreased the absorbance strength over the catalyst; it was measured at 15 min intervals. 15 min time gap, the dye solution was taken out and centrifuged for 1000 rpm to remove the catalyst from the dye solution and measured in UV-Visible spectroscopy. The dissociated dye absorbance was calculated for the both dyes. The extent of the degradation was monitored by measuring the absorbance before and after degradation at 667 nm and 497 nm for methylene blue and Congo red respectively.

3.9.1 Catalyst dose

For the optimization purpose, catalyst dose from 0.02gm to 0.1gm with ranging of 0.02gm and 0.01g to 0.15 with ranging 0.03 was taken per 25ml of methylene blue and the Congo red respectively at constant value of the other parameters then the catalytic degradation efficiency was calculated for each dyes.

3.9.2 Initial concentration of the dye

To investigate the effect of initial concentration of the dyes on catalytic degradation efficiency, different initial concentration for both dyes (1, 5, 10, 15, 20 and 25 ppmfor CR; 1, 5, 10, 15, and 20 for MB) were used by taking other parameters as constant like catalyst dosage, exposure time, and pH.

3.9.3 Exposure time

For the investigation of the total reaction time required for the total degradation of the methylene blue and Congo red nine trials were taken by range of 15 minute gap (15-135 minute). The other parameters optimized (catalyst dose, initial concentration and pH) before were applied.

3.9.4 pH of the dyes

To study the effects of pH, for the degradation of both dyes the other parameters optimized were kept constant and optimum pH was investigated by varying pH from 4 to 14 values for both (MB and CR) dyes.

3.10 Determination of Degradation Percentage

To study the photocatalytic degradation activity of nanoparticles and nanocomposite, a series dye solution having different concentrations was prepared for both dyes. 100ml of the dye solution was taken in a beaker along with different quantity of nanoparticles and nanocomposite and kept under sunlight along with continuous stirring. The absorbance was taken after definite time intervals and the degradation efficiency for both dyes calculated by:

$$\text{Degradation percentage } \% = \frac{\boldsymbol{Ao - At}}{\boldsymbol{Ao}} \times 100 \qquad (10)$$

Where Ao - initial absorbance of the dyes solution before exposed to sun light, $\mathbf{A_t}$ is absorbance of dyes solution at time t.

3.11 Kinetic Study

In this study, all measurements were done under optimized experimental conditions. In doing this, calibration curves were constructed for both dyes, which are aimed at calculating the concentrations of the dyes after degradation at a different time interval. Then constant concentrations (initial concentration with high degradation efficiency) were prepared for the both dyes and the extent of the degradation studied with in 15 minute intervals. Then the concentration of the dyes was calculated by applying Beer-Lambert law.

$$A = \varepsilon bc \qquad (11)$$

Where $\boldsymbol{A}$ is absorbance, $\boldsymbol{\varepsilon}$ is molar absorptivity constant, b is path length and $\boldsymbol{c}$ is concentration.

This equation is related with $y = mx + b$ and from absorbance versus concentration data slop (m) was calculated and used to calculate the concentration after degradation. Finally pseudo-zero order, pseudo first order, and pseudo second order kinetics was investigated according to equation 5, 6, and 7 listed above in literature review part.

3.12 Instrumental Calibration

The standard stock solutions of dyes were taken for the calibration of the instrument for dyes used for the experiment. Firstly 1000 ppm of stock solution of each dye was prepared and an intermediate solution containing 100 ppm was prepared in 500 ml volumetric flask. Then the intermediate standards were diluted with distilled water to obtain five working standards of each dye of interested for calibration purpose. Calibration of the instrument purpose was to study the linearity of the instrument response and also calculation of the remaining concentration of the organic dyes after degradation in investigating the kinetics of the degradation experiment.

3.13 Study on Catalyst Reusability

The usability of the catalyst was investigated in the degradation process under identical experiment conditions (at optimum concentration of the dye solution, catalyst dose and exposure time). After the completion of the reaction, the catalyst was separated by centrifugation from the reaction mixture, and washed with ethanol and water; finally dried and reused for four consecutive cycles.

CHAPTER FOUR

4 RESULTS AND DISCUSION

4.1 Characterization of the Biosynthesized Nanoparticle

4.1.1 Ultra violate-Visible spectroscopy Analysis

The UV– vis absorption spectra of the Co_3O_4 NPs, PANI, and Co_3O_4/PANI nanocomposite were investigated using UV-VIS spectroscopy between the wavelength range 200–800 nm and their spectra are given in Figure 9 (a, b, and c), respectively. The formation of biosynthesized Co_3O_4 NP was identified by distinct absorbance peaks at 218 and 690 nm (Figure 9a). These peaks correspond to the O^{2-} to Co^{2+} and O^{2-} to Co^{3+} charge transfer processes, indicating the dual oxidation states of cobalt elements are [72, 73]. In the UV-vis absorption spectrum of PANI (Figure 9b), the absorption band at 268 nm corresponds to the transition from π to π^* of C = C in the benzenoid rings, while the band in the 400–450 nm range indicates the π to polaron transitions [74, 75]. A blue shift observed in the UV region in Figure 9c may result from a strong interaction between the orbitals of the metal oxide d and π orbitals within the polymeric material. The UV-Vis absorption spectrum of the PANI-Co_3O_4 nanocomposites (Figure 9c) showed a red shift in the UV region at 230 nm, showing an intense peak compared to Co_3O_4 and PANI individually. This change indicates a clear combination of Co_3O_4 within the PANI conducting matrix, highlighting the formation of the PANI-Co_3O_4 nanocomposite with enhanced optical properties and structural characteristics.

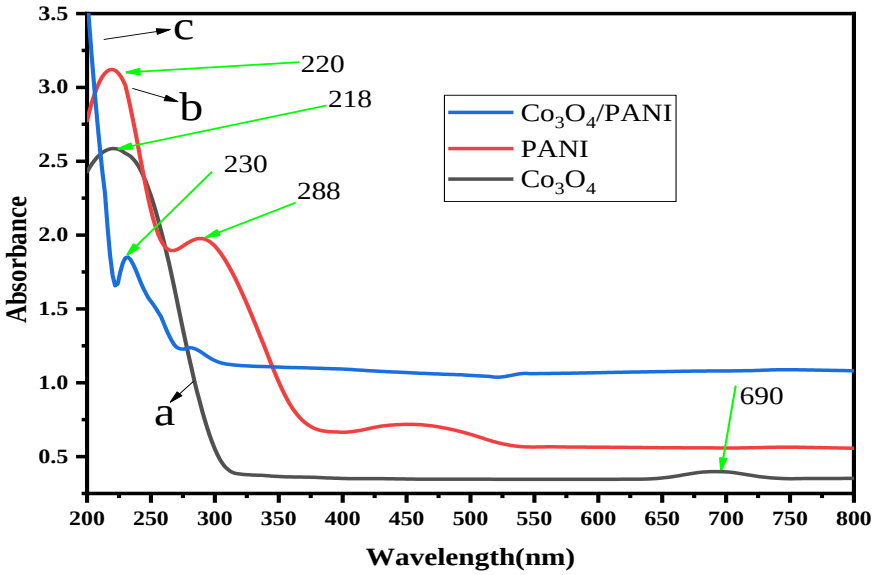

Figure 9: UV-Vis absorption spectra of (a) Co_3O_4 NP (Black curve), (b) pure PANI (Red curve), and (c) Co_3O_4/PANI (blue curve).

The energy band gap spectra of the Tauc plot of Co_3O_4 NP, PANI and PANI-Co_3O_4 NCs are shown in Figure 10 (a, b, and c), respectively. The band gap is the minimum energy needed for an electron to be excited from the top of valence band to the bottom of conduction band. Once that minimum energy is reached then the sample can start absorbing light and electrons are excited from valence band to the conduction band. The band gap energy of biosynthesized Co_3O_4 NPs and PANI-Co_3O_4 nanocomposites, and synthesized PANI was estimated by applying the Tauc model. The optical band gap can be determined using the well-known Tauc relation from Equation (11) [76].

$$(\alpha h\nu)^n = A(h\nu - E_g) \qquad (12)$$

Where, A is the constant related to material, α is the absorption coefficient in cm^{-1} , hν is photon energy in eV, Eg is the band gap energy in eV, and n is the constant that is equal to 2, 1/2, 2/3, and 1/3 for allowed direct, allowed indirect, forbidden direct, and forbidden indirect transitions, respectively. In this case, n =1/2 for the determination of the optical band gap of Co_3O_4 NPs, PANI and PANI-Co_3O_4 nanocomposites. The following formula [77] can be used to determine the band gap energy of the material (Eg).

$$E_g(ev) = \frac{1240}{\lambda(\mathrm{nm})} \qquad (13)$$

Where, Eg is bang gap energy (eV), λ is the wave length in (nm), corresponding to the absorption edge. The band gap was estimated by extrapolating the linear region in the plot of $(\alpha h\nu)^{1/2}$ versus hν (photon energy) as shown in the Figure 10 (a, b, and c).

The determined band gap energy results of biosynthesized Co_3O_4 Nps, PANI, and Co_3O_4 /PANI Nanocomposite by using tauic plot are shown in Table 3

Table 3: Optical band gap energy values for Co_3O_4 Nps, PANI, and Co_3O_4/PANI Nanocomposites.

Sample	E_{g1}	E_{g2}	E_{g3}
Co_3O_4 Nps	1.69	3.93	-
PANI	1.57	3.1	4.12
Co_3O_4/PANI	3.26	3.80	5.3

From these results it is known that the E_g values of Co_3O_4/PANI have been reduced than that of CO_3O_4 Nps and PANI. This is due to the change in the particle size concerning the surface modification with PANI.

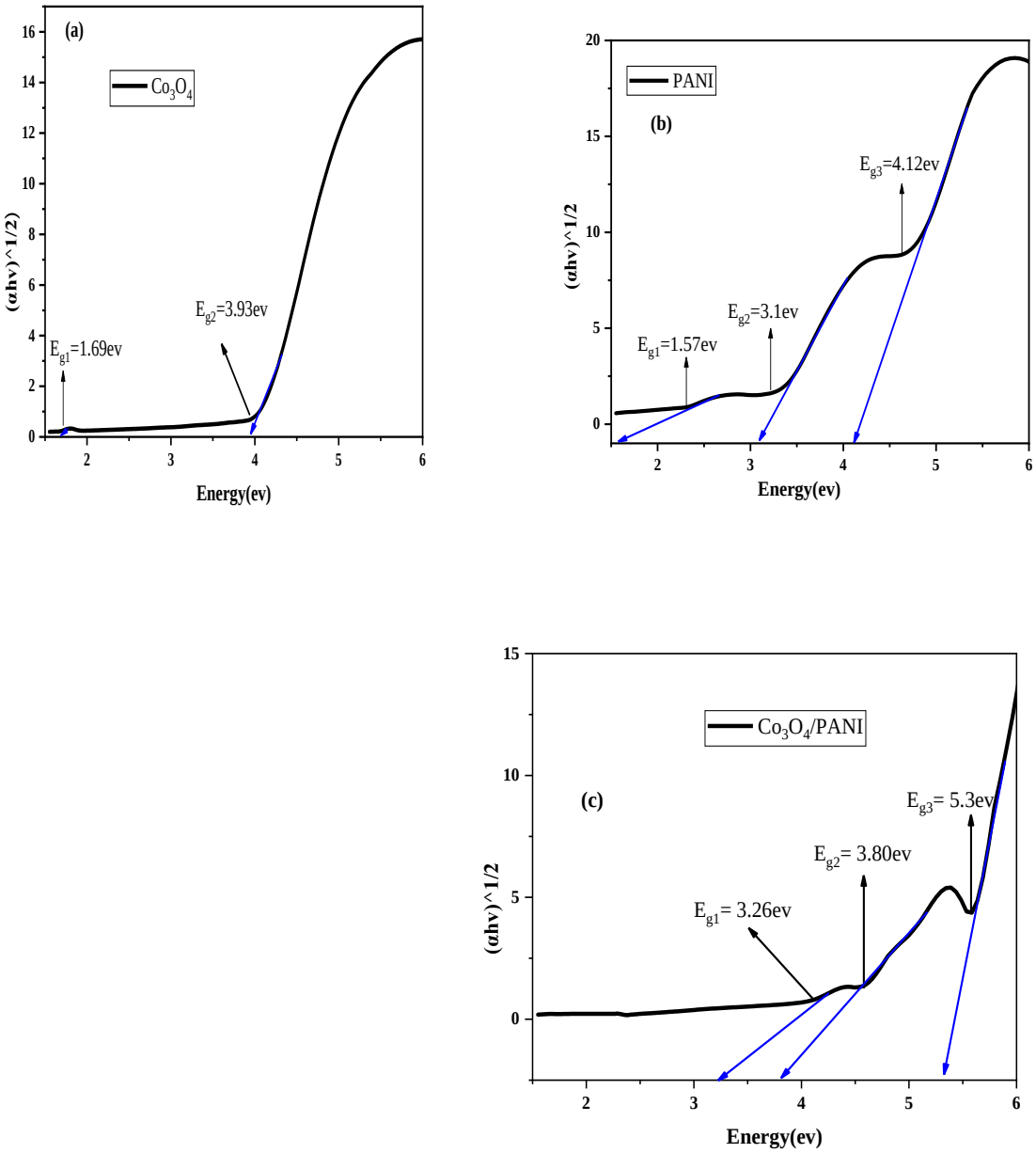

Figure 10: Tauc plot band gap energy of (a) Co_3O_4 Nps, (b) PANI and (c) Co_3O_4/PANI NCs**.**

4.1.2 Fourier Transform infrared (FT-IR) spectra analysis

The synthesized materials were characterized by Fourier transform infrared (FT-IR) spectroscopy in the transmission range of 4000 to 400cm^{-1} as shown in Figure 11, for identification of functional groups present. The FTIR analysis (Figure 11a) for the leaf extract of *Vernonia amygdalina* shown that the wavenumber absorption of 3470 cm^{-1} represented the hydroxyl (-OH) group, while at 2931 cm^{-1} characterized the C-H absorption. The peak observed at 1631 and 1402 cm^{-1} indicates C = C stretching and O-H bending of carboxylic acid, respectively. The band at 1173 cm^{-1} corresponds to the C-O stretching of an aromatic ester. The peak at 1018 cm^{-1} is due to the C-N stretching vibration of amines [78, 79]. In Figure 11(b), shown by blue line, the prominent band observed at approximately 3326 cm^{-1} indicate the O–H stretching attributed to the presence of surface adsorbed water molecules in Co_3O_4 nanoparticles. The prominent absorption bands at 555 cm^{-1} and 648 cm^{-1}, attributed to the stretching vibrations of the metal-oxygen bond corresponding to (Co^{3+} - O) and (Co^{2+}- O) vibrations, respectively. These observations provide strong evidence for the successful preparation of Co_3O_4 NP. Furthermore, a recent study noted the presence of two distinct bands indicates the vibrations of Co^{3+} and Co^{2+} ions occupying octahedral and tetrahedral sites, respectively, further confirming the structural composition of the synthesized materials[72].

Additional, peaks at 1628 cm^{-1} and 1401 cm^{-1} shows C=C, and C–N stretching vibration respectively which may obtained from when plant biomolecules used as reducing, capping, and stabilizing agent during preparation of Co_3O_4 NPs [36,80].

In Figure 11c the typical FT-IR spectra of pure PANI (red curve), the characteristic band formed at 3368 corresponding to O–H stretching vibration in pure PANI, which can also be observed in Co_3O_4 /PANI composite as shown in Figure 11d (black curve) [81].

The peak at 1622 cm^{-1} is due to the C=C stretching vibration of the quinoid rings ((N=Q=N)).The 1403 cm^{-1} peak can be attributed to the C=C stretching vibration of the benzenoid ring (N-B-N) and bands at 1119 cm^{-1} is due to the C–N stretching of a secondary aromatic amine [82, 83].

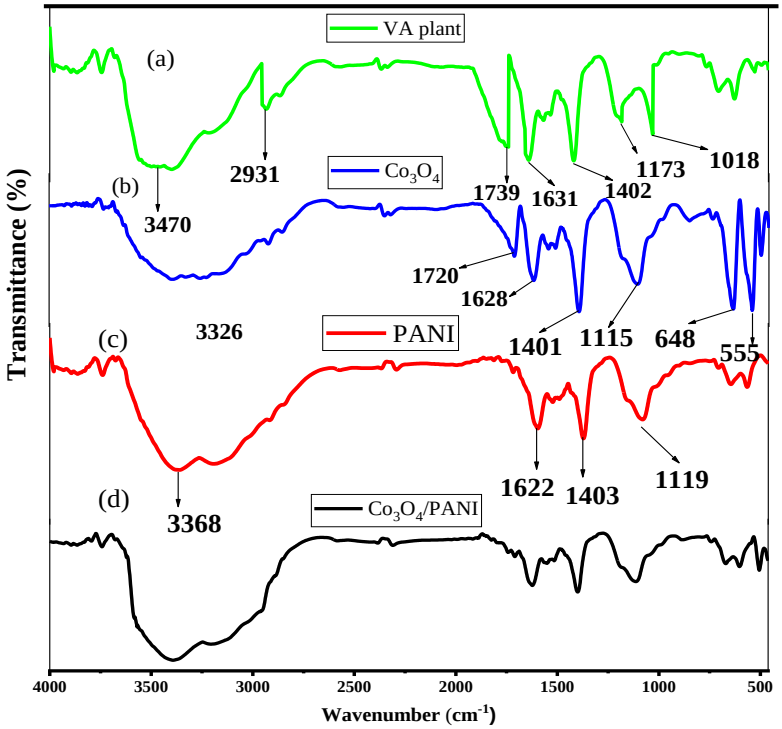

Figure 11: FT-IR spectra of (a) VA plant, (b) Co_3O_4 Nps; (c) PANI and (d) Co_3O_4/PANI NCs

4.1.3 Scanning Electron microscopy (SEM) analysis

The surface morphologies of Co_3O_4 nanoparticle, PANI, and Co_3O_4-PANI was investigated using scanning electron microscopy (SEM) in Figure 11. Figure 11(a) depicts the SEM image of biosynthesized Co_3O_4 NPs with an aggregated flower-like nanostructure. Figure 11(b) shows the non-uniform, rough, and closely packed irregular granular micrographs for pure PANI [75]. Previous studies have examined that the successful formation of the PANI-MO NCs can be attributed to ionic interaction between the PANI and the metal oxides NPs. Similar reports on the successful formation of metal oxide/carbon nanomaterial based nanocomposites have been attributed to either π-π or electrovalent interaction between the metal oxide and the carbon based nanomaterial [84]. The micrograph of Co_3O_4/PANI illustrated in Figure 11(c) indicates that PANI-Co_3O_4 NCs exhibit higher porosity and superior particle dispersion compared to Co_3O_4

nanoparticles and PANI powder. The enhanced porosity and particle dispersion are promising properties that can potentially enhance the catalytic performance of the synthesized nanoparticles. Formation of PANI coating over Co_3O_4 could be linked to electrostatic interaction between PANI and surface charge on Cobalt oxide nanoparticles. Thus, the SEM results indicated the successful surface functionalization of the Co_3O_4 nanoparticles with PANI.

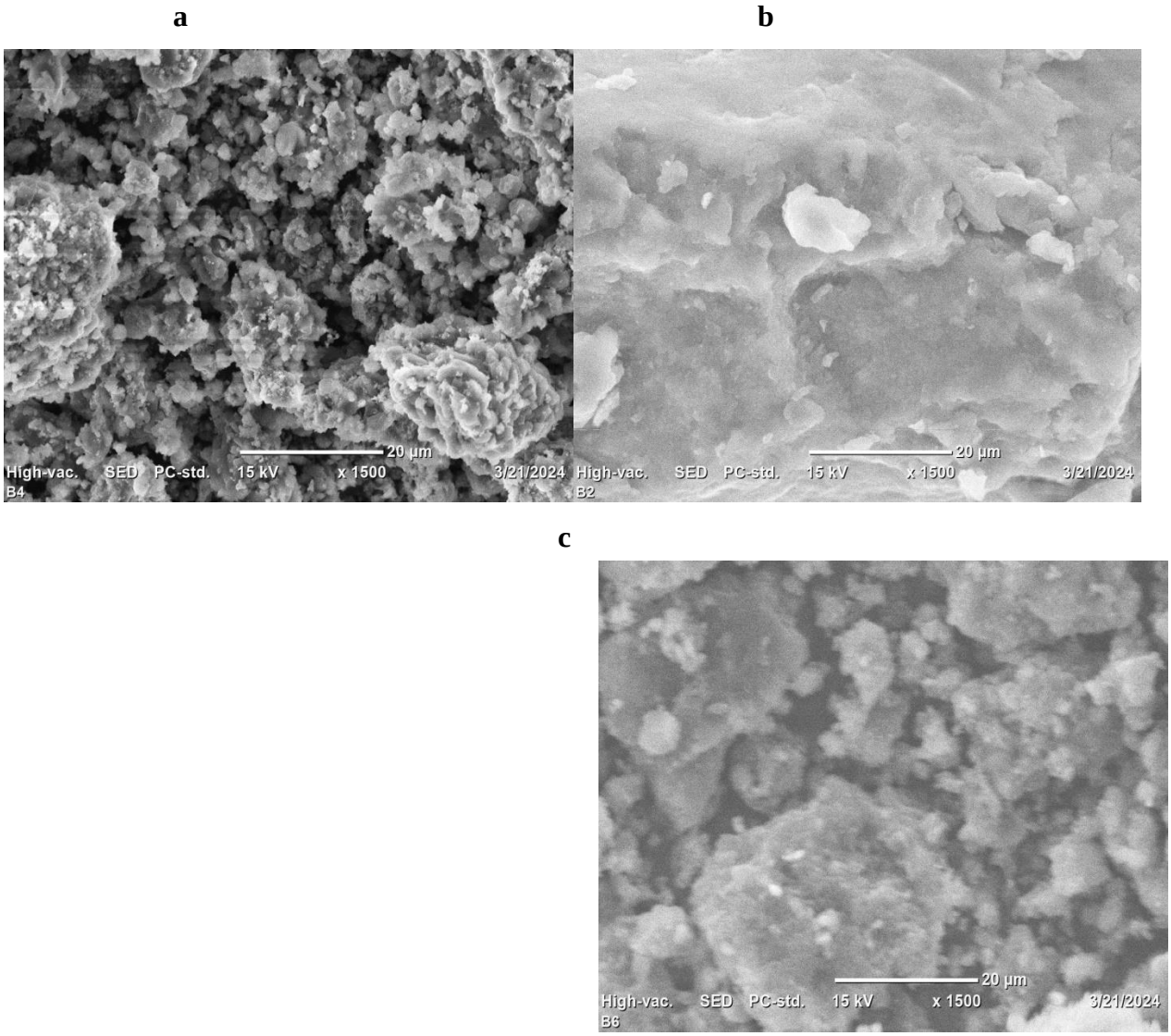

Figure 12: SEM images of (a) Co_3O_4 NP, (b) PANI powder, and (c) Co3O4/PANICo_3O_4 NCs**.**

4.1.4 X-ray diffraction (XRD) analysis

X-ray diffraction (XRD) measurements were used to determine the phase purity and crystal structure of the synthesized PANI, Co_3O_4 NPs, and Co_3O_4/PANI NCs. Figure 13 shows the XRD patterns of PANI, Co_3O_4 nanoparticles and Co_3O_4 /PANI nanocomposites. The XRD pattern of PANI (figure y (a)) exhibits broad peaks at 2θ =25.15 (110) due to the characteristic chain of PANI. The higher intensity peak 2θ =25.22(110) correspond to planes with higher atomic scattering factors or greater crystalline order [85]. The diffraction peaks of Co_3O_4 (figure yb) nanoparticles appearing at 2θ = 29.99°(220), 36.74°(311), 38.05°(222), 44.62°(400) 59.26° (511), and 65.31°(440) of the planes. The obtained Co_3O_4 nanoparticles peaks are well-coincided with the cubic structure of standard JCPDS (Joint committee on powder Diffraction Standards) card number 042-1467 [72]. In the case of PANI coated Co_3O_4 nanoparticles, the peaks at 2θ are shown at the plane of 25.33° (110)), which suggest the contribution peaks of PANI. The peaks at the angle of 36.73°, 44.76° and 59.25°, and 65.17° plane of 311,400,511 and 440 respectively are the corresponding peaks of cobalt oxide nanoparticles (Figure yc). The average crystal sizes (D) determined was found to be 19.25 nm, 8.24 nm and 11.03 nm for Co_3O_4 NPs, PANI powder, and PANI-Co_3O_4 NCs respectively by applying Debye Scherer's equation. According to above analysis, all the diffraction peaks can be indexed to the lattice planes of PANI and Co_3O_4, suggesting that the synthesized nanostructures had purity without containing other compounds or impurities and the formation of Co_3O_4/PANI NCs. The XRD patterns in Figure13 showed broad peaks, indicating the existence of nanocrystals. To determine the crystallinity of the synthesized nanostructures, the crystallite size was estimated using the Scherer formula. Estimation of the interplanar spacing in the lattice and the crystallite size of synthesized materials was calculated by using Braggs law and the Debye-Scherrer equation respectively [81], from Equations (14 and 15) given below which reveals a relationship between X-ray diffraction peak broadening and crystallite size.

$$n\lambda = 2d\sin\theta \qquad (14)$$

Whereas, n is an integer, λ is the XRD wavelength for Cu Kα (0.154 nm) and θ is the angle between the incident ray and the scattering planes.

$$D = k\lambda/\beta\cos\theta \qquad (15)$$

where D is the crystallite size (nm), k is Scherer shape factor constant for an average crystallite (0.9) depending on the miller index of the reflecting plane and the shape of the crystal, λ is the XRD wavelength (nm), β is the full width at half maximum (FWHM) of crystallite peak (measured in radians) and θ is Bragg's angle (°) of the XRD peak.

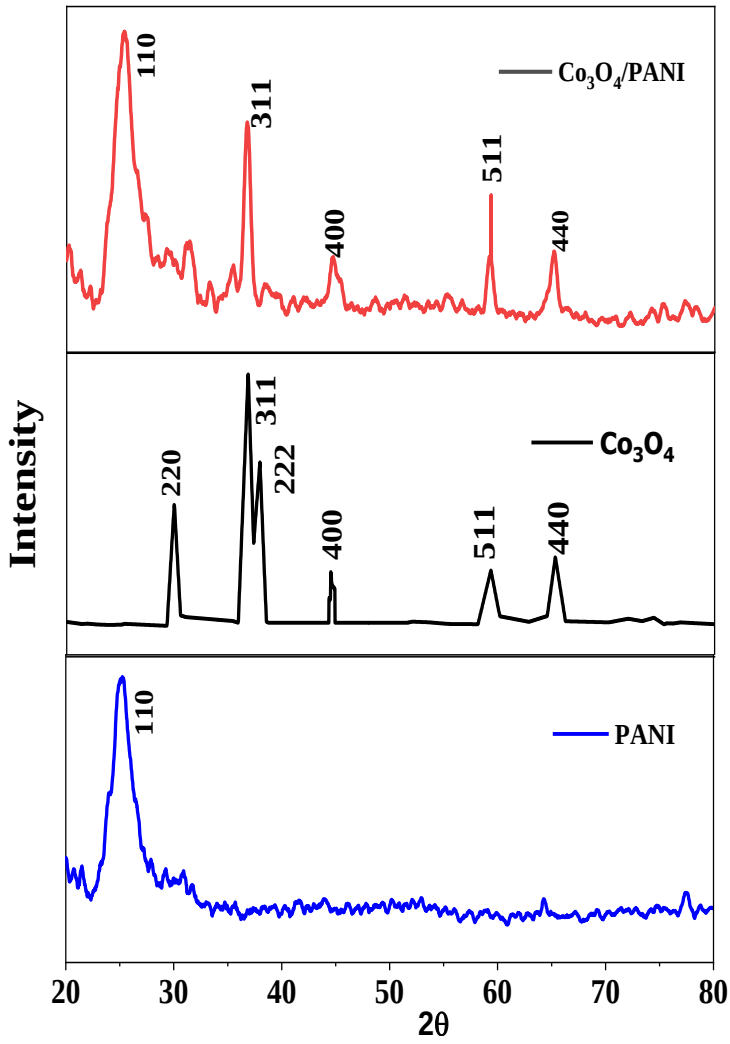

Figure 13: XRD patterns of (a) PANI powders (b) Co_3O_4 nanoparticles, and (c) Co_3O_4/PANI NCs

Table 4: X-ray diffraction (XRD) analysis of Co_3O_4 Nanoparticle

No	2θ (°)	d-spacing(nm)	FWHM (°)	Miller indices (h k l)	Crystallite size nm (nm)
1	29.99	0.2977	0.67201	220	15.62832
2	36.74	0.2444	0.87353	311	10.25075
3	44.62	0.2029	0.66663	400	12.54964
4	38.05	0.2363	0.42353	222	19.04975
5	59.26	0.1558	1.13287	511	32.84949
6	65.31	0.1427	0.96549	440	25.2654

Average crystalline size =19.25nm

Table 5: X-ray diffraction (XRD) analysis of PANI

No	2θ (°)	d-spacing (nm)	FWHM (°)	Miller indices (hkl)	Crystallite size (nm)
1	25.24	0.352566	2.68515	110	8.24nm

Table 6: X-ray diffraction (XRD) analysis of Co_3O_4/PANI Nanocomposite

No	2θ (°)	d-spacing (nm)	FWHM (°)	Miller indices (h k l)	Crystallite size (nm)
1	25.33	0.351	2.34083	110	3.41
2	36.73	0.2444	0.64737	311	13.86
3	44.76	0.2023	0.81535	400	10.52
4	59.25	0.1558	0.61067	511	5.95
5	65.17	0.1430	0.94698	440	21.45

Average crystalline size =11.03nm

4.2 Photocatalytic Degradation Analysis of Co_3O_4 NPs and Co_3O_4/PANI NCs

The degradation of the selected organic dyes using Co_3O_4 NPs and Co_3O_4/PANI was studied by determining the optimum experimental parameters such as pH, initial dye concentration, catalyst dose, and exposure time under natural sunlight irradiation. Observation of the decay in color and calculation of the percentage of degradation using the absorbance value before and after degradation were implemented as the preliminary screening of the occurrence of the degradation.

4.3 Experimental Parameters for Photocatalytic Degradation

4.3.1 Effect of Catalyst dose

Figure 14 indicates the optimum dose of the prepared photocatalyst for the degradation of both dyes. For Methylene blue, degradation efficiency increased up to a dose of 0.06g (88.27%) in NPs, (90.84%) in NCs and then decrease. Also, the degradation efficiency of Congo red increases up to a catalyst dose of 0.09 g (93.13%) and 88.29% in NCS and NPs respectively. Lowering the catalyst dose below the optimum value reduces degradation because more light passes through the reaction medium and small amount of light is used in the photocatalytic reaction [57]. This increase in degradation efficiency is due to the generation of more active sites on the photocatalysts surface as the dose of catalyst increases which consequently increases the number of hydroxyl and superoxide radicals. It has been reported that in heterogeneous photocatalytic reactions, the photo catalytic degradation of dye is in proportion with the loaded catalyst and it increases as a result of an increase in the amount of loaded catalyst [64]. As the catalyst dose increased further, the percent of degradation decreased due to light penetration inhibition, and less hydroxyl radical will be generated. Aggregation of nanoparticles at high catalyst doses may also contribute to a lower degradation percentage by reducing the number of active sites and producing fewer active radicals [86].

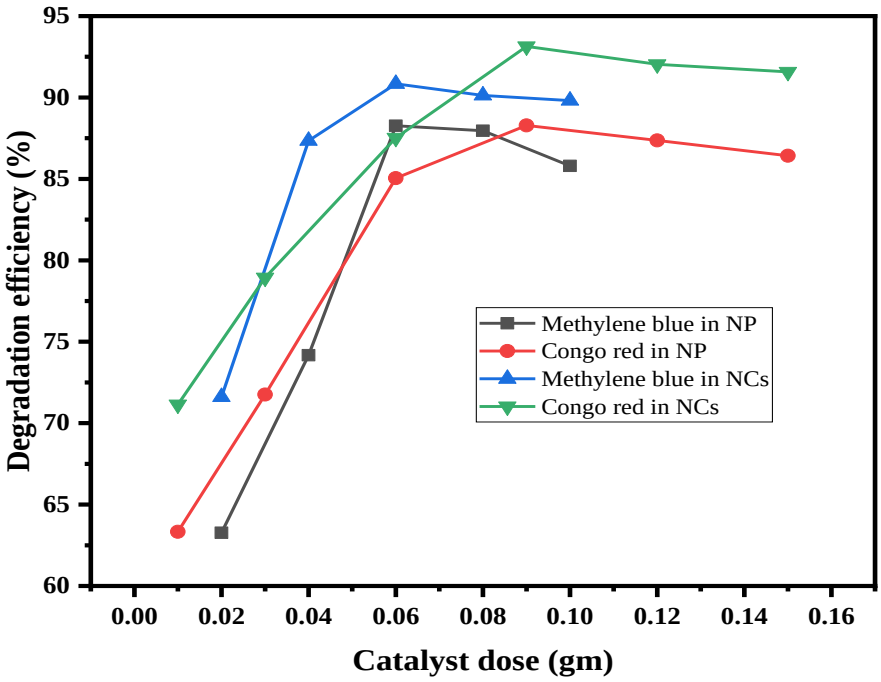

Figure 14: Effect of catalytic dose on Methylene blue and Congo red degradation, with initial concentration 10 ppm for MB and 15ppm for Congo red in NP and NCs.

4.3.2 Effect of initial concentration

The optimization of the initial dye concentrations was performed by varying the initial dye concentrations (1ppm to 25ppm for Congo red with a gap of 5 ppm and 1ppm to 20ppm for Methylene blue with a gap of 5ppm) as presented in Figure 15. The degradation efficiency increases up to 15ppm for Congo red, whereas for Methylene blue, it increases up to 10ppm. Then, after these two optimum values of initial concentrations, the efficiency decreased. The increment in degradation with increasing the initial dye concentration is just because more dyes are available for degradation, as well as several monolayer of adsorbed dye formed and this will be true up to the optimum point. This decrease in degradation efficiency with increasing initial dye concentration above the optimum value is primarily due to a large amount of adsorbed dye, which may also inhibit reactions between dye molecules and reactive radicals [54]. Since the excessive dye concentration may hinder light penetration into the solution, fewer photons can reach the photocatalyst surface [55].

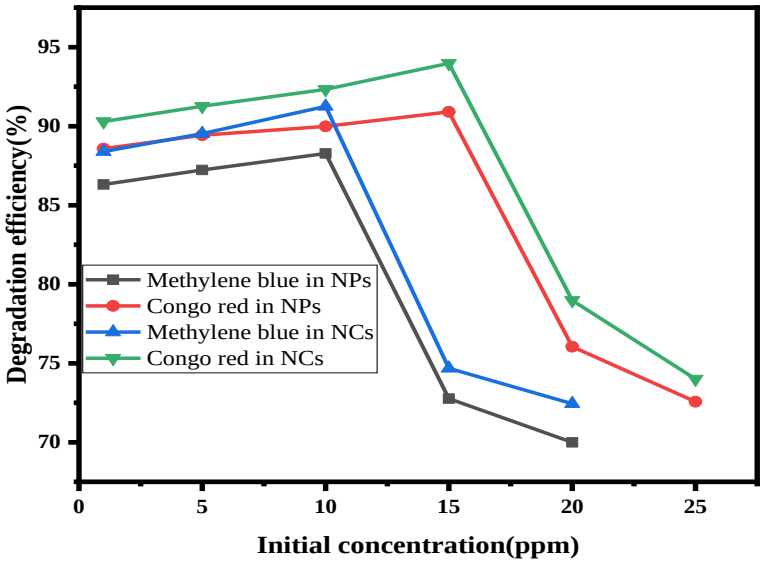

Figure 15: Effect of initial concentration on Methylene blue and Congo red degradation, catalyst dose: 0.06 g/25 mL for Methylene blue and 0.09 g/25mL for Congo red.

4.3.3 Effect of exposure time

The effect of exposure time on the photo degradation of both dyes was investigated and shown in Figure 16 the degradation efficiency of both MB and CR increases up to 105 minute and 90 minute respectively then seems to maintain constant efficiency above the optimum point for both dyes. This result shows the time required (90 for CR and 105 minute for MB) for the degradation of the dyes within the efficiency of the prepared photocatalyst. When the time of total degradation of the dyes reached the degradation efficiency of the photocatalyst, further exposition time would not be useful as it couldn't bring more results beyond the efficiency of the catalyst.

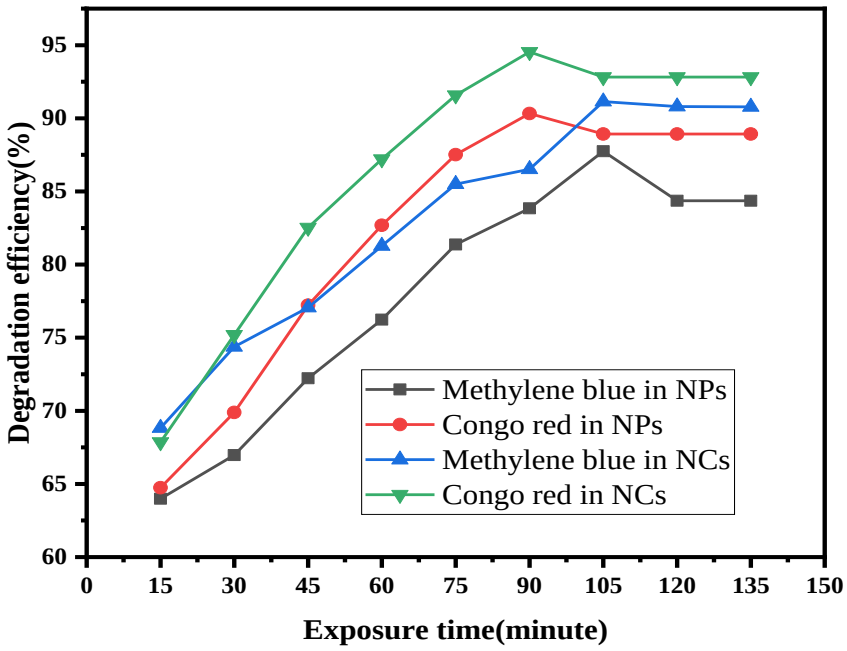

Figure 16: Effects of exposition time for degradation of MB and CR, Catalyst dose: 0.06 gm/25ml for MB, Co; 10ppm and 0.09 gm/25ml for CR, with Co 15 ppm**.**

4.3.4 Effect of pH

The optimum pH for both of the dyes was investigated and summarized in Figure 17. The pH at which maximum degradation efficiency (91.66%) was obtained for Methylene blue was 10 (the pH of the mixture of the dye and catalyst itself) in NCs and 89.60% in NPs. The maximum degradation efficiency obtained at this pH is attributed to the effects of the pH in facilitating the adsorption between the dyes and the photocatalysts. The optimum pH value for the degradation of Congo red was 8. This Congo- red molecule is also an anionic dye (two negatively charged sulphonate groups per molecule). The high degradation percent at pH 8 (93.69%) in NCS is due to the possible adsorption between the dye and the catalyst and 90.79% in Co_3O_4 NPs. In this acidic medium, the catalyst is positively charged through protonation, and for both of the dyes, adsorption is possible here because of the electrostatic force of attraction between the dyes and the catalyst. This decrease in degradation efficiency above the optimum pH is mainly due to the electrostatic repulsion between the negatively charged group of the CR dyes and the negatively charged surface of the catalyst through the addition of the base [56].

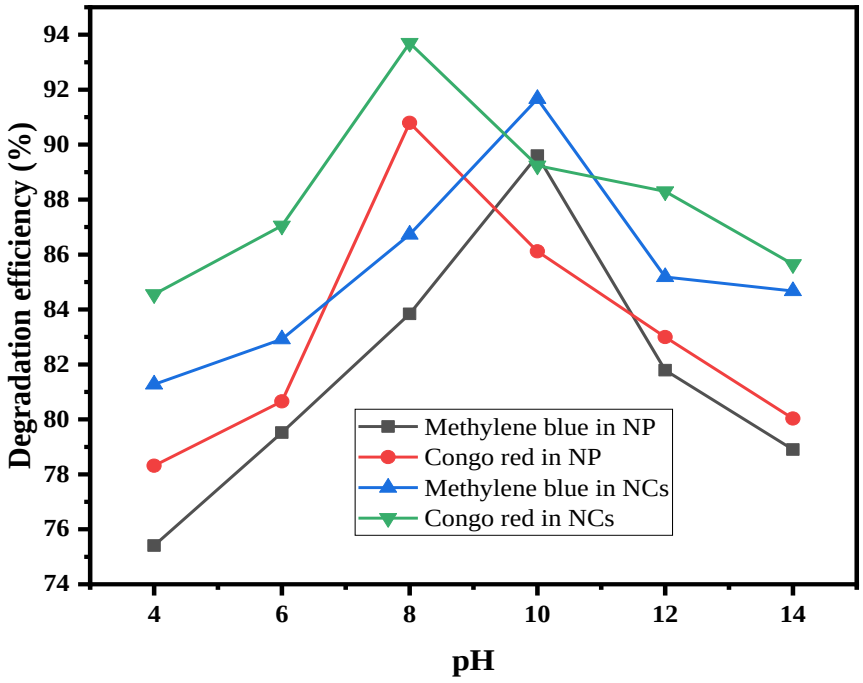

Figure 17: Effect of pH for degradation of MB and CR by Co_3O_4/PANI NCs, Catalyst dose: 0.0.6 g/25 mL Co; 10 ppm, Contact time 105 min for MB and 0.09 g/25 mL, Co; 15ppm, Contact time 90min for CR.

4.4 Kinetic study

The study of kinetics of photocatalytic degradation is necessary; as it contains several information about the reaction occurred at the surface of photocatalyst. Kinetic models have been exploited to test the experimental data and to determine the mechanism of adsorption and its potential rate-controlling step that include mass transfer and chemical reaction.

In this study, three kinetics models (pseudo zero-order, pseudo first-order, and pseudo second order) have been tasted in order to predict photodegradation rate of the dyes. The photodegradation pseudo kinetics experiments were carried outs at different exposition time in range from 15 to 135 minute on 10ppm and 15ppm initial concentration of MB and CR respectively and other experimental parameters optimized were kept constant.

To investigate the pseudo kinetics, calibration curves were constructed as shown Figure 18, which was aimed at calculating the concentration of the dyes after degradation at different time intervals. Data for calibration of MB and CR dyes recorded on appendix 6.

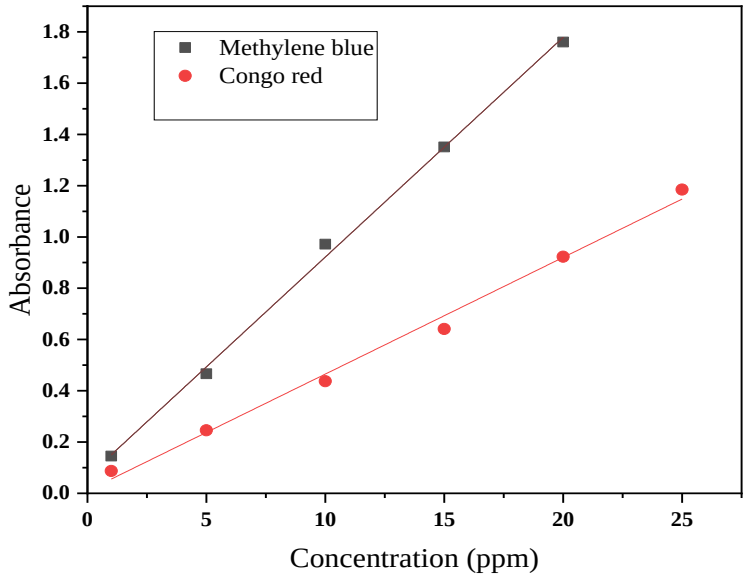

Figure 18: Calibration curve for Methylene blue and Congo red

The final concentration of the both dyes were calculated using their respective calibration curve by taking slop value of each dyes (**ε**=0.0857 for MB and **ε**= 0.0455 for CR) and the other quantities used for investigating the pseudo kinetics were calculated and accumulated in the following table.

Table 7: Kinetic study For MB and CR Co_3O_4 in NPs

Dye	**C_0(ppm)**	**A_t**	**C_t**	**Time(min)**	$\boldsymbol{C0 - Ct}$	$\ln(Co/Ct)$	$\frac{1}{Ct} - \frac{1}{C0}$
MB	10	0.35	4.08	15	5.916	0.895	0.144
		0.321	3.74	30	6.254	0.982	0.167
		0.27	3.15	45	6.849	1.155	0.217
		0.231	2.69	60	7.304	1.311	0.271
		0.181	2.11	75	7.888	1.555	0.373
		0.157	1.83	90	8.168	1.697	0.445
		0.119	1.38	105	8.611	1.974	0.620
		0.152	1.77	120	8.226	1.729	0.463
		0.152	1.77	135	8.226	1.729	0.463
CR	15	0.226	4.96	15	10.04	1.106	0.134
		0.193	4.23	30	10.77	1.265	0.169
		0.146	3.2	45	11.8	1.544	0.245
		0.111	2.43	60	12.57	1.820	0.344
		0.08	1.75	75	13.25	2.148	0.504
		0.062	1.36	90	13.64	2.400	0.668
		0.071	1.55	105	13.45	2.269	0.578
		0.071	1.55	120	13.45	2.269	0.578
		0.071	1.55	135	13.45	2.269	0.578

Table 8: Kinetic study For MB and CR in Co_3O_4/PANI NCs

Dye	**C_0(ppm)**	**A_t**	**Ct**	**Time(min)**	$\boldsymbol{C0 - Ct}$	$\boldsymbol{\ln(Co/Ct)}$	$\boldsymbol{\frac{1}{Ct} - \frac{1}{C0}}$
MB	10	0.303	3.53	15	6.47	1.041	0.183
		0.249	2.9	30	7.1	1.237	0.244
		0.223	2.6	45	7.4	1.347	0.284
		0.182	2.12	60	7.88	1.551	0.371
		0.141	1.64	75	8.36	1.807	0.509
		0.131	1.52	90	8.48	1.883	0.557
		0.086	1	105	9	2.302	0.9
		0.089	1.04	120	8.96	2.263	0.861
		0.089	1.04	135	8.96	2.263	0.861
CR	15	0.206	4.52	15	10.48	1.199	0.154
		0.159	3.49	30	11.51	1.458	0.219
		0.112	2.46	45	12.54	1.807	0.339
		0.082	1.8	60	13.2	2.120	0.488
		0.054	1.18	75	13.82	2.542	0.780
		0.035	0.76	90	14.24	2.982	1.249
		0.046	1.01	105	13.99	2.698	0.923
		0.046	1.01	120	13.99	2.698	0.923
		0.046	1.01	135	13.99	2.698	0.923

4.4.1 Pseudo Zero- Order Kinetic

The linearized pseudo zero- order kinetics equation is shown on equation 6 and plot for both dyes shown Figure 19 and 20. As stated in equation 6, plot of Co-Ct versus time gives pseudo zero-order kinetics, where Co is initial concentration before degradation while Ct is concentration at time t on the degradation. In the pseudo zero- order kinetics study a high correlation coefficient close to unity 0.993 and 0.984 for MB in NPs and NCS respectively compared to the other model, which indicates, it seems to follow pseudo zero- order kinetics. A pseudo zero- order reaction is, thus, observed for saturation coverage on the surface of the photocatalyst and photodegradation rate is independent of the dye concentration. The slope of the graph is the zero-order rate constant, which is 0.03083. The correlation coefficient and rate constant are shown in table 9.

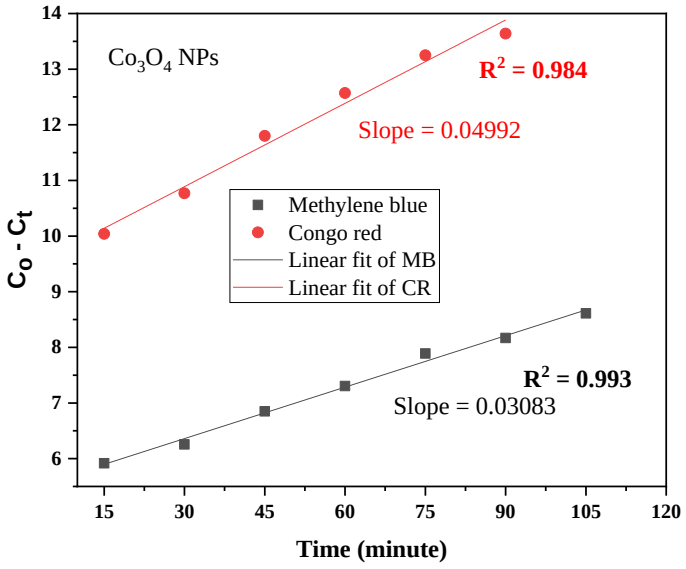

Figure 19: Pseudo zero- order kinetics model for Methlyene blue and Congo red in Co_3O_4

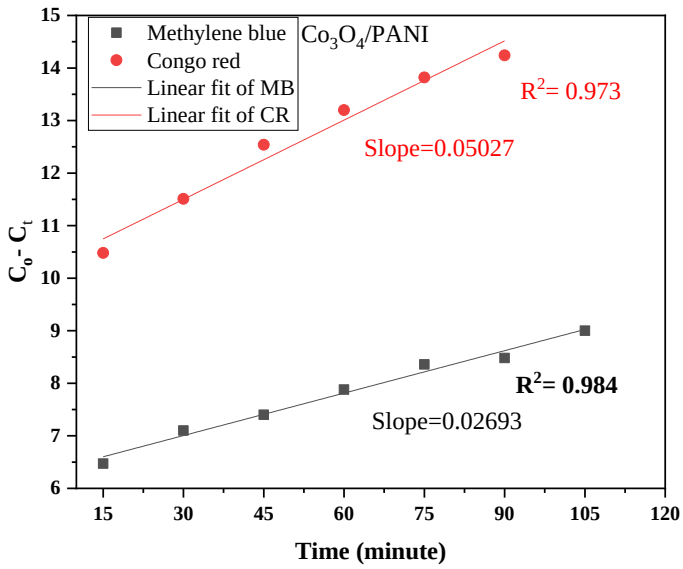

Figure 20: Pseudo zero- order kinetics model for MB and CR in Co_3O_4/PANI NCs

4.4.2 Pseudo First- Order Kinetic

The linearized pseudo first- order kinetics equation is shown on equation 7 and plot for both dyes shown Figure 21 and 22. As stated in equation 7, plot of $\ln(Co/Ct)$ versus time gives pseudo first-order kinetics, where Co is initial concentration before degradation while Ct is concentration at time t on the degradation.

Figure 21 and 22: was graph constructed for MB and CR in investigating the pseudo first-order kinetics. The most linear graph with the correlation coefficient of 0.992 and 0.991 was obtained for Congo red in NPs and NCs respectively. It indicates the heterogeneous photocatalytic degradation of CR on the surface Co_3O_4 NPs follow pseudo first-order kinetics i.e. rate of degradation and concentration of the dyes are directly proportional. The Pseudo first-order rate constant of the photodegradation was found to be $1.789*10^{-2}$ and $2.377*10^{-2}$ for NPs and NCS respectively which can be seen from table 9.

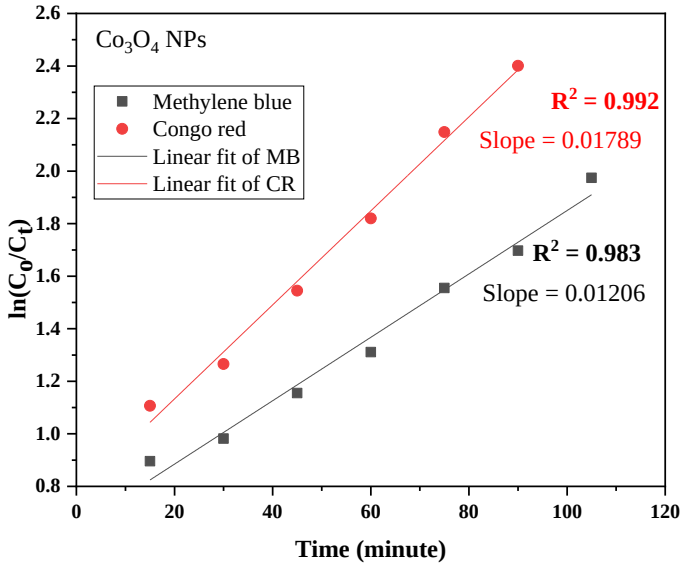

Figure 21: Pseudo first- order kinetics model for Methlyene blue and Congo red in Co_3O_4 NPs

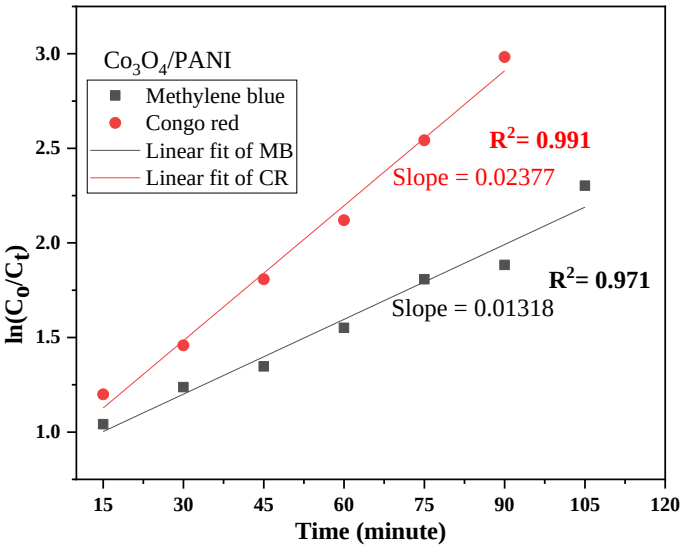

Figure 22: Pseudo first- order kinetics model for MB and CR in Co_3O_4/PANI NCs

4.4.3 Pseudo second-order kinetics

Pseudo second- order kinetics was also investigated for the photocatalytic degradation of the MB and CR dyes. The linearized equation for plotting of the graph is found equation 7. According to

the equation plot $\frac{1}{Ct} - \frac{1}{Co}$ versus time t displays pseudo second-order kinetic graph. Figure 23 and 24 shows graph of pseudo second-order kinetics of both dyes. Relative to the other pseudo kinetics models (Pseudo first and second- order), the correlation coefficient of this figure is less for both dyes (0.945 and 0.930 in NPs, 0.89 and 0.88 in NCs for CR and MB respectively) which suggests, that the photocatalytic degradation of both dyes not fit this model.

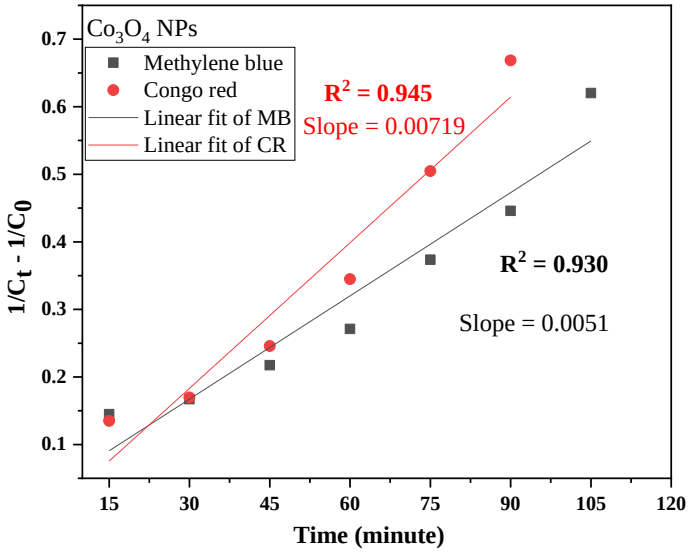

Figure 23: Pseudo second- order kinetics model for Methlyene blue and Congo red in NPs

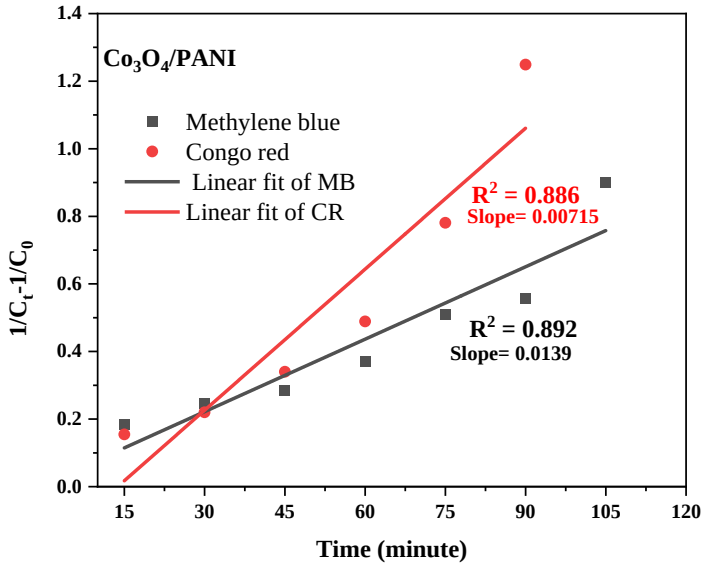

Figure 24: Pseudo second- order kinetics model for MB and CR in Co_3O_4/PANI NCs

Table 9: Rate constant (k) and correlation coefficient (R^2) calculated for kinetics model in Co_3O_4 NPs and Co_3O_4/PANI nanocomposites

Types of models	Dyes				
	Methylene blue			Congo red	
		K	R^2	K	R^2
pseudo zero – order	Co_3O_4	0.03083	0.993	0.04992	0.984
	Co_3O_4/PANI	0.02693	0.984	0.05027	0.973
pseudo first – order	Co_3O_4	0.01206	0.983	0.01789	0.992
	Co_3O_4/PANI	0.01318	0.971	0.02377	0.991
pseudo second – order	Co_3O_4	0.0051	0.930	0.00719	0.945
	Co_3O_4/PANI	0.0139	0.892	0.00715	0.886

4.5 Study on Catalyst Reusability

Reusability and stability of the catalysts are vital for determining the performance of catalyst as the active and stable catalyst could considerably decrease the cost of the process. Reusability of Co_3O_4 NPs and Co_3O_4/PANI NCs for the degradation of MB and CR was tasted at optimized condition with the four times. Figure 25 and appendix 7 showed that the reusability study of the Co_3O_4 NPs and Co_3O_4/PANI NCs which possess the good recyclability for the degradation of the both dyes. Thus, it was concluded that Co_3O_4 NPs and Co_3O_4/PANI NCs could be used several times in various chemical ractions as an active catalyst. The results suggest that these green synthesized materials obtained in this study were relatively stable and could be successfully used as efficient catalyst with a slight decrease in the degradation rate fore more than four times.

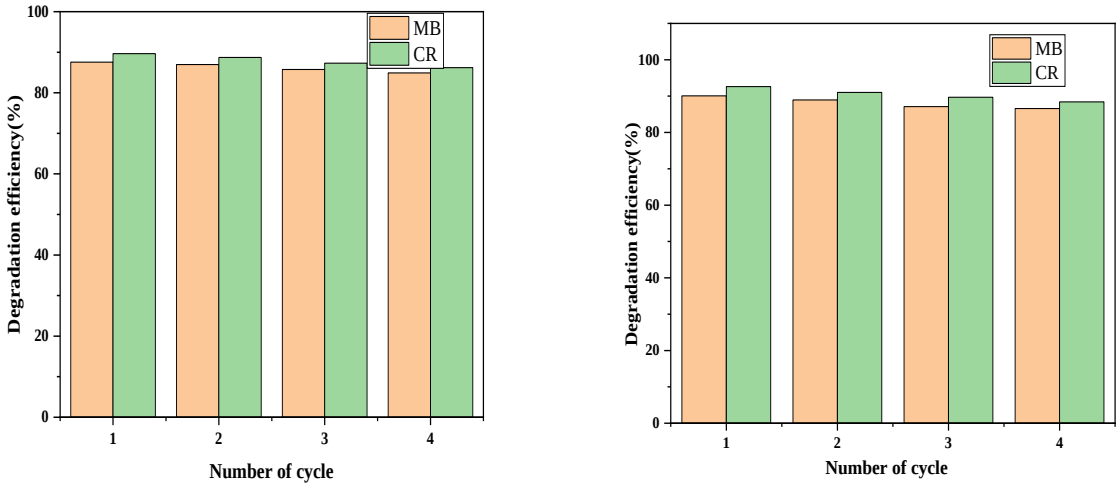

Figure 25: the reusability study of the Co_3O_4 NPs and Co_3O_4/PANI NCs for the degradation of the both dyes (MB and CR).

CHAPTER FIVE

5 CONCLUSION AND RECOMMENDATION

5.1 Conclusion

Under this study, PANI, Co_3O_4 NPs, and Co_3O_4/PANI were synthesized successfully by green synthetic method and applied for photocatalytic degradation of Methylene blue and Congo red. The characterization of synthesized material was done by analytical techniques such as XRD, FT-IR, UV-Visible and SEM. The FT-IR spectra revealed characteristic peak of Co_3O_4, PANI and functional group present in vernonia amaygdalina leaf extract that are assumed as reducing and cupping agents in the preparation of Co_3O_4 NPs. XRD patterns examine the crystalline size of Co_3O_4 NPs; PANI powder and PANI-Co_3O_4 nanocomposites were successfully estimated using the Scherer formula with an average particle size 19.25nm, 8.24nm and 11.03nm for Co_3O_4 NPs, PANI powder, and Co_3O_4/PANI NCs, respectively. Morphological investigations indicated that have low aggregated flower-like structure of Co_3O_4 NPs, non-uniform, rough, and closely packed irregular granular micrographs of PANI, and porous irregular structure of Co_3O_4/PANI nanocomposites. Furthermore, from UV-Visible spectra of synthesized PANI, Co_3O_4 NPs and Co_3O_4/PANI NCs band gap energy were obtained and the band gap energy values of Co_3O_4 NP were 1.69 and 4.93eV. Furthermore, the band-gap energies of PANI were found to be 1.57eV and 3.12eV with an additional band of 4.12eV. However, the band gap energy values of the PANI-Co_3O_4 nanocomposites were found to be 3.26eV and 3.80eV with an additional band of 5.3eV. From photocatalytic degradation study, it is possible conclude that this synthesized Co_3O_4 NPS and Co_3O_4/PANI has efficiency to degrade MB and CR under natural sun light irradiation. The photocatalytic degradation was found to be strongly dependent on photocatalyst dose, initial concentration, pH, and exposure time of the dyes. Maximum degradation was found to be 93.69% in Co_3O_4/PANI NCS and 90.79% in Co_3O_4 NP under optimum conditions (catalyst dose 0. 0.09 gm, initial concentration 15ppm, exposure time 90 min, and pH of 8) and 91.66% and 89.60% in Co_3O_4/PANI NCS and 90.79% in Co_3O_4 NP under optimum condition (catalyst dose 0.06 gm, initial concentration 10 ppm, exposure time 105min, and pH of 10) for CR and MB respectively. In general Co_3O_4/PANI NCS shows more degradation efficiency than Co_3O_4 NPs due to mutual interactions between inorganic semiconductors and conducting polymers give rise

to interesting properties. The kinetic study indicates photocatalytic degradation of a MB follows pseudo zero- order kinetics whereas CR follows pseudo first order kinetics.

5.2 Recommendation

The following recommendations were made for future work. There are areas that need more work and not covered by this study:

- ✓ For future study a characterization of Co_3O_4, PANI and Co_3O_4/PANI nanocomposite that will give full information in order to investigate the particle size and more detail morphology of the prepared samples, so the sample should be characterized by Transmission Electron Microscopy (TEM). The elemental distribution of the synthesized samples also should be characterized by energy dispersive X-Ray (EDX).
- ✓ Application of Co_3O_4 NPs and Co_3O_4/PANI as a photocatalyst in degrading other commercial dye in wastewater treatment has to be used in future study.
- ✓ The way to monitor light intensity under solar radiation and studying the effect of light intensity also needs further studies.
- ✓ The effect of temperature on photodegradation under solar radiation; how to monitor and studying its effect has to be also included in future study.

REFERENCE

1. Mirzaei, H. and Darroudi M. “Zinc oxide nanoparticles: biological synthesis and biomedical application,” *ceramics international*. **2013**, 43(1), 907-914.
2. Arruda, S. C. C., Silva, A. L. D., Galazzi, R. M., Azevedo, R. A., & Arruda, M. A. Z. Nanoparticles applied to plant science: a review. *Talanta*, **2015,** 131, 693-705.
3. Albanese, A., Tang, P. S., & Chan, W. C. The effect of nanoparticle size, shape, and surface chemistry on biological systems. *Annual review of biomedical engineering*. **2012**, 14(1), 1-16.
4. Hasan S. ‘‘A Review on Nanoparticles: Their Synthesis and Types Biosynthesis and Mechanism. ’’ Research *journal of recent sciences*, **2015**, 4, 1-3.
5. Agarwa ,H.I ,Kumar S.V and Rajeshkumar S ., ‘‘A review on green synthesis of zinc oxide nanoparticles an eco-friendly approach, ’’ *Resource –efficient Technologies* .**2017**, 3406-413
6. Dhanya, R., K. S. Suganthi, and K. S. Rajan. “Studies on Scale-up of Synthesis of ZnO Nanoparticles.” *Asian Journal of Chemistry*. **2014**, 26(14), 4273.
7. Gusmão, K. A. G., Gurgel, L. V. A., Melo, T. M. S., & Gil, L. F. Adsorption studies of methylene blue and gentian violet on sugarcane bagasse modified with EDTA dianhydride (EDTAD) in aqueous solutions: kinetic and equilibrium aspects. *Journal of environmental management*, **2013**, 118, 135-143.
8. Madkour, L. H., & Madkour, L. H. Introduction to nanotechnology (NT) and nanomaterials (NMs). *Nanoelectronic materials: fundamentals and applications*, **2019**, 1-47.
9. Isaacoff, B. P., & Brown K. A. “Progress in top-down control of bottom-up assembly.” *Nano Letters* **2017**, 17(11), 6508-6510.
10. Gherbi, B., Laouini, S. E., Meneceur, S., Bouafia, A., Hemmami, H., Tedjani, M. L. ... & Menaa, F. Effect of pH value on the bandgap energy and particles size for biosynthesis of ZnO nanoparticles:Efficiency for photocatalytic adsorption of methyl orange. *Sustainability*, **2022**, *14*(18), 11300.
11. Yang, W., et al. “Crop phenomics and high-throughput phenotyping: past decades, current challenges, and future perspectives.” *Molecular Plant*, **2020**, 13(2), 187-214.

12. Mohammadlou, M., Maghsoudi, H. and Jafarizadeh-Malmiri, H. “A Review on Green Silver Nanoparticles Based on Plants: Synthesis, Potential Applications and Eco-Friendly Approach.” *International Food Research Journal*, **2016**, 232, 446-463.
13. Nazir, A., Raza, M., Abbas, M., Abbas, S., Ali, A., Ali, Z. ... & Iqbal, M. Microwave assisted green synthesis of ZnO nanoparticles using Rumex dentatus leaf extract: photocatalytic and antibacterial potential evaluation. *Zeitschrift für Physikalische Chemie*, **2022,** 236(9), 1203-1217.
14. Kumari, S., & Sarkar, L. A review on nanoparticles: structure, classification, synthesis & applications. *Journal of Scientific Research*, **2021,** 65(8), 42-46.
15. Ikhuoria, E. U., Omorogbe, S. O., Sone, B. T., & Maaza, M. Bioinspired shape controlled antiferromagnetic Co_3O_4 with prism like-anchored octahedron morphology: A facile green synthesis using Manihot esculenta Crantz extract. *Science and Technology of Materials*, **2018,** 30(2), 92-98.
16. Mohammadi, S. Z., Lashkari, B., & Khosravan, A. Green synthesis of Co_3O_4 nanoparticles by using walnut green skin extract as a reducing agent by using response surface methodology. *Surfaces and Interfaces*, **2021**, 23, 100970.
17. Hafeez, M., Shaheen, R., Akram, B., Haq, S., Mahsud, S., Ali, S., & Khan, R. T. Green synthesis of cobalt oxide nanoparticles for potential biological applications. *Materials Research Express*, **2020**, 7(2), 025019.
18. Suresh, S., Vennila, S., Anita Lett, J., Fatimah, I., Mohammad, F., Al-Lohedan, H. A., ... & Rafie Johan, M. Star fruit extract-mediated green synthesis of metal oxide nanoparticles. *Inorganic and Nano-Metal Chemistry*, **2022**, 52(2), 173-180.
19. Yadav, S., Rani, N., & Saini, K. (2022, February). A review on transition metal oxides based nanocomposites, their synthesis techniques, different morphologies and potential applications. *IOP Conference Series: Materials Science and Engineering*, **2022**, 1225(1), 012004.
20. Venkatreddy, J., Reddy, N., Reddy, B. R., Naresh, P., Lavanya, B., Prasad, M. V. N. ... & Inamdar, H. K. Green synthesis of Co_3O_4/polyaniline nanocomposites: Structural, morphological and conductivity studies. *AIP Conference* **20202,** 2269, 030094.

21. Shahabuddin, S., Sarih, N. M., Ismail, F. H., Shahid, M. M., & Huang, N. M. Synthesis of chitosan grafted-polyaniline/Co_3O_4 nanocube nanocomposites and their photocatalytic activity toward methylene blue dye degradation. *RSC advances*, **2015**; 5(102), 83857-83867.
22. Bouras, D., Rasheed, M., Barille, R., & Aldaraji, M. N. Efficiency of adding DD3+ (Li/Mg) composite to plants and their fibers during the process of filtering solutions of toxic organic dyes. *Opt. Mater*. **2022**, 131, 112725.
23. Siddiqui, V. U., Ansari, A., Ansari, M. T., Akram, M. K., Siddiqi, W. A., Alosaimi, A. M. ... & Rafatullah, M. Optimization of facile synthesized ZnO/CuO nanophotocatalyst for organic dye degradation by visible light irradiation using response surface methodology. *Catalysts* **2021**, 11, 1509.
24. Nuengmatcha, P., Chanthai, S., Mahachai, R., & Oh, W. C. Sonocatalytic performance of ZnO/graphene/TiO_2 nanocomposite for degradation of dye pollutants (methylene blue, texbrite BAC-L, texbrite BBU-L and texbrite NFW-L.) under ultrasonic irradiation. *Dyes and Pigments*. **2016**, 134,487-497.
25. Salami, R., Amini, M., Bagherzadeh, M., & Hosseini, H. Vanadium supported on spinel cobalt ferrite nanoparticles as an efficient and magnetically recoverable catalyst for oxidative degradation of methylene blue. *Applied Organometallic Chemistry*, **2019**, 33(10), e5127.
26. Yang, K., Li, Y., Zheng, H., Luan, X., Li, H., Wang, Y. ... & Xia, Y. Adsorption of Congo red with hydrothermal treated shiitake mushroom. *Materials Research Express*, **2019**, 7, 015103.
27. Higgins, M. M., González, M. T., & Rojas, J. Enhanced X-RAYS degradation of methylene blue in the presence of gold microspheres. *Radiation Physics and Chemistry*.**2019**, 156, 73-80.
28. Zamora-Ledezma, C., Negrete-Bolagay, D., Figueroa, F., Zamora-Ledezma, E., Ni, M., Alexis, F., & Guerrero, V. H. Heavy metal water pollution: A fresh look about hazards, novel and conventional remediation methods. *Environmental Technology & Innovation*, **2021**, *22*, 101504.

29. Babar, U. D., Garad, N. M., Mohite, A. A., Babar, B. M., Shelke, H. D., Kamble, P. D., & Pawar, U. T. Study the photovoltaic performance of pure and Cd-doped ZnO nanoparticles prepared by reflux method. *Materials Today: Proceedings*, **2021**, 43, 2780-2785.
30. Shamaila, S., Sajjad, A. K. L., Farooqi, S. A., Jabeen, N., Majeed, S., & Farooq, I. Advancements in nanoparticle fabrication by hazard free eco-friendly green routes. *Applied Materia*, *Today* **2016**, 5, 150–199.
31. Iravani, S., & Varma, R. S. Sustainable synthesis of cobalt and cobalt oxide nanoparticles and their catalytic and biomedical applications. *Green Chemistry*, **2020**, 22, 2643–2661.
32. Hanif, M. A., Kim, Y. S., Akter, J., Kim, H. G., & Kwac, L. KFabrication of robust and stable N-doped ZnO/single-walled carbon nanotubes: characterization, photocatalytic application, kinetics, degradation products, and toxicity analysis. *ACS Omega* **2023**, 8, 16174–16185.
33. Maeda, K., Ishimaki, K., Tokunaga, Y., Lu, D., & Eguchi, M. Modification of Wide-Band-Gap Oxide Semiconductors with Cobalt Hydroxide Nanoclusters for Visible-Light Water Oxidation. *Angewandte Chemie International Edition*, **2016**, 55, 8309–8313.
34. El-Shamy, O. A., & Deyab, M. A. The most popular and effective synthesis processes for Co3O4 nanoparticles and their benefit in preventing corrosion. *Zeitschrift für Physikalische Chemie*. **2023**, 273(3), 333-350.
35. Kaur, D., Kaur, N., & Chopra, A. A comprehensive review on phytochemistry and pharmacological activities of Vernonia amygdalina. *Journal of Pharmacognosy and Phytochemistry* **2019**, 8(3), 2629-2636.
36. Safdar, A., Mohamed, H. E. A., Hkiri, K., Muhaymin, A., & Maaza, M. Green synthesis of cobalt oxide nanoparticles using hyphaene thebaica fruit extract and their photocatalytic application. *Applied Sciences*, **2023**, 13(16), 9082.
37. Haridevi, M., Prabu, S., Mohanraj, K., Arun, A., & Kayalvizhi, M. (2018). Synthesis and Characterization Polyaniline/Cobalt Oxide Nanocomposite by Chemical Oxidation Method. *Nanoscale Reports.* **2018**, 1, 9-20.

38. Imran, H. J., Hubeatir, K. A., Aadim, K. A., & Abd, D. S. Preparation methods and classification study of nanomaterial: A review. In *Journal of Physics: Conference Series*. **2021**, 1818(1). IOP Publishing.
39. Khalid, K., Tan, X., Mohd Zaid, H. F., Tao, Y., Lye Chew, C., Chu, D. T. ... & Chin Wei, L. Advanced in developmental organic and inorganic nanomaterial: a review. *Bioengineered*. **2020**, 11(1), 328-355.
40. Khan, I., Saeed, K., & Khan, I. Nanoparticles: Properties, applications and toxicities. .*Arabian journal of chemistry* **2019**, 12 (7), 908-931.
41. S. Kandasamy and R. "Sorna Prema. Methods of synthesis of nano particles and its applications." *Journal of Chemical and Pharmaceutical Research*, **2015**, 7(3), 278-285
42. Singh, J.et al. "Green synthesis of metals and their oxide nanoparticles: Applications for environmental remediation." *Journal of Nanosbiotechnology*, **2018**, 16(1), 1–24.
43. Shafey, A. M. E. Green synthesis of metal and metal oxide nanoparticles from plant leaf extracts and their applications: A review. *Green Processing and Synthesis*, **2020**, 9(1), 304–339
44. Rajeswari, V. D., Khalifa, A. S., Elfasakhany, A., Badruddin, I. A., Kamangar, S., & Brindhadevi, K. Green and ecofriendly synthesis of cobalt oxide nanoparticles using Phoenix dactylifera L: Antimicrobial and photocatalytic activity. *Applied Nanoscience*, **2023**, 13(2), 1367-1375.
45. Bibi, I., Nazar, N., Iqbal, M., Kamal, S., Nawaz, H., Nouren, S. ... & Abbas, M. Green and eco-friendly synthesis of cobalt-oxide nanoparticle: characterization and photo-catalytic activity. *Advanced Powder Technology*.**2017**, 28(9), 2035-2043.
46. Shanker, U., Jassal, V., & Rani, M. Catalytic removal of organic colorants from water using some transition metal oxide nanoparticles synthesized under sunlight. *RSC advances*, **2016**, 6, 94989
47. Pagar, T., Ghotekar, S., Pagar, K., Pansambal, S., & Oza, R. A review on bio-synthesized Co_3O_4 nanoparticles using plant extracts and their diverse applications. *Journal of Chemical Reviews*, **2019**, 1, 260-270

48. Govindasamy, R., Raja, V., Singh, S., Govindarasu, M., Sabura, S., Rekha, K. ... & Thiruvengadam, M. Green synthesis and characterization of cobalt oxide nanoparticles using Psidium guajava leaves extracts and their photocatalytic and biological activities. *Molecules*, **2022,** 27, 5646.
49. M. C. Sonawane and N. S. Warude, "Review Article: Review of Cobalt Oxide Nanoparticles: Green Synthesis, Biomedical Applications, and Toxicity Studies". **2022**, 4 (4). 331–345.
50. Dessie, Yilkal, Sisay Tadesse, and Rajalakshmanan Eswaramoorthy. "Surface Roughness and Electrochemical Performance Properties of Biosynthesized α-MnO_2/NiO-Based Polyaniline Ternary Composites as Efficient Catalysts in Microbial Fuel Cells." *Journal of Nanomaterials*. **2021**, 1-21.
51. Zhu, J., Zhang, Z., Zhao, S., Westover, A. S., Belharouak, I., & Cao, P. F. Single-ion conducting polymer electrolytes for solid-state lithium–metal batteries: design, performance, and challenges. *Advanced Energy Materials*. **2021** 11(14), 2003836.
52. Bedre, M. D., Basavaraja, S., Deshpande, R., Sawle, B. D., Lagashetty, A. K., Govindraj, B., & Venkataraman, A. Preparation and characterization of polyaniline-NiO nanocomposites via interfacial polymerization. *Journal of Metallurgy and Materials Science*, **2012**, 2(3), 3943.
53. Kumar, H., Luthra, M., Punia, M., & Singh, R. M. Co_3O_4/PANI nanocomposites as a photocatalytic, antibacterial and anticorrosive agent: Experimental and theoretical approach. *Colloid and Interface Science Communications*. **2021**, 45, 100512.
54. Mohammadi, S. Z., Safari, Z., & Madady, N. Synthesis of Co_3O_4@ SiO_2 Core/Shell–Nylon 6 magnetic nanocomposite as an adsorbent for removal of congo red from wastewater. *Journal of Inorganic and Organometallic Polymers and Materials.* **2020**, 30, 3199-3212.
55. Miclescu, A., & Wiklund, L. Methylene blue, an old drug with new indications. *J Rom Anest Terap Int*. **2010**, 17(1), 35-41.
56. Noori, M. T., Tiwari, B. R., Ghangrekar, M. M., & Min, B. Azadirachta indica leaf-extract-assisted synthesis of CoO–NiO mixed metal oxide for application in a microbial fuel cell as a cathode catalyst. *Sustainable Energy & Fuels*, **2019** 3, 3430–3440.

57. Akpan, U. G., & Hameed, B. H. Parameters affecting the photocatalytic degradation of dyes using TiO_2-based photocatalysts: a review. *Journal of hazardous materials* **2009**, 170(2-3), 520-529.
58. Gowland, D.C.A.; Robertson, N.; Chatzisymeon, E. "Photocatalytic Oxidation of Natural Organic Matter in Water." *Water* **2021**, 13, 288.
59. Feng, T., Feng, G. S., Yan, L., & Pan, J. H. One-Dimensional Nanostructured TiO_2 for Photocatalytic Degradation of Organic Pollutants in Wastewater. *International Journal of Photoenergy* **2014**.
60. Harun, N. H., Rahman, M. A., Kamarudin, W. W., Irwan, Z., Muhammud, A., Akhir, N. E. F. M., & Yaafar, M. R. Photocatalytic degradation of Congo red dye based on titanium dioxide using solar and UV lamp. *Journal of Fundamental and Applied Sciences* 10.1S **2018**, 10 (1S), 832-846.
61. Kumar, A., & Pandey, G. A review on the factors affecting the photocatalytic degradation of hazardous materials. *Material Sci & Eng Int J*. **2017**, 1(3), 106–114.
62. Azad, K., & Gajanan, P. J. C. S. J. Photodegradation of methyl orange in aqueous solution by the visible light active Co: La: TiO_2 nanocomposite. *Chem. Sci. J*. **2017**, 8(3), 1000164-1000174.
63. Cavigli, L., Bogani, F., Vinattieri, A., Faso, V., & Baldi, G. Volume versus surface-mediated recombination in anatase TiO2 nanoparticles. *Journal of Applied Physics*. **2009**, 106(5).
64. Coleman, H. M., Vimonses, V., Leslie, G., & Amal, R. Degradation of 1, 4-dioxane in water using TiO_2 based photocatalytic and H_2O_2/UV processes. *Journal of Hazardous Materials*, **2007**, 146(3), 496–501.
65. Ahmed, S., Rasul, M. G., Brown, R., & Hashib, M. A. Influence of parameters on the heterogeneous photocatalytic degradation of pesticides and phenolic contaminants in wastewater: a short review. *Journal of environmental management*. **2011**, 92(3), 311-330.

66. Qingshan, Y. A. N. G., Yongjin, L. I. A. O., & Lingling, M. A. O. Kinetics of photocatalytic degradation of gaseous organic compounds on modified TiO_2/AC composite photocatalyst. *Chinese Journal of Chemical Engineering*, **2012**, 20(3), 572-576.
67. Irani, M., Mohammadi, T., & Mohebbi, S. Photocatalytic degradation of methylene blue with ZnO nanoparticles; a joint experimental and theoretical study. *Journal of the Mexican Chemical Society*. **2016**, 60(4), 218-225.
68. Kiwumulo, H. F., Muwonge, H., Ibingira, C., Lubwama, M., Kirabira, J. B., & Ssekitoleko, R. T. Green synthesis and characterization of iron-oxide nanoparticles using Moringa oleifera: a potential protocol for use in low and middle income countries. *BMC Research Notes*, **2022**, 15(1), 1-8.
69. Gemechu, Fikadu Aaga & Sisay Tadesse Anshebo. "Green synthesis of highly efficient and stable copper oxide nanoparticles using an aqueous seed extract of Moringa stenopetala for sunlight-assisted catalytic degradation of Congo red and alizarin red s." *Heliyon.***2023**, 9(5).
70. Mohammad Shafiee, M. R., Sattari, A., Kargar, M., & Ghashang, M .MnO_2/Cr_2O_3/PANI nanocomposites prepared by in situ oxidation polymerization method: optical and electrical behaviors. *Journal of Applied Polymer Science*, **2019**, 136, 47219,
71. Venkatreddy, J., Reddy, N., Reddy, B. R., Naresh, P., Lavanya, B., Prasad, M. V. N., ... & Inamdar, H. K. Green synthesis of Co_3O_4/polyaniline nanocomposites: Structural, morphological and conductivity studies. In *AIP Conference Proceedings*, **2020**, 2269(1).
72. Chelliah, P., Wabaidur, S. M., Sharma, H. P., Jweeg, M. J., Majdi, H. S., AL. Kubaisy, M. M. R., ... & Lai, W. C. Green synthesis and characterizations of cobalt oxide nanoparticles and their coherent photocatalytic and antibacterial investigations. *Water* **2023**, 15(5), 910.
73. Khalaji, A. D. Synthesis, characterization and optical properties of Co_3O_4 nanoparticles. *Asian J.Nanosci. Mater.* **2019**, 2, 186-190.
74. Diggikar, R. S., Deshmukh, S. P., Thopate, T. S., & Kshirsagar, S. R. Performance of polyaniline nanofibers (PANI NFs) as PANI NFs-silver (Ag) nanocomposites (NCs) for energy storage and antibacterial applications. *ACS Omega* **2019**, 4, 5741–5749.

75. Mazzeu, M. A. C., Faria, L. K., Cardoso, A. D. M., Gama, A. M., Baldan, M. R., & Gonçalves, E. S. Structural and morphological characteristics of polyaniline synthesized in pilot scale. *Journal of Aerospace Technology and Management*, **2017**, 9, 39-47.
76. Xaba, T., Mokgoera, L., Nate, Z., Shumbula, P. M., & Africa, S. synthesis and characterization of cubic structured cobalt oxide nanoparticles capped with topo through the decomposition of bis (n-cyclohexyl-1-naphthaldehydato) cobalt (ii) complex as a single source precursor. *Dig* J Nanomaterials.Biostructures, **2019**, 13(4), 1141-1147
77. Ezhilarasi, A. A., Vijaya, J. J., Kaviyarasu, K., Kennedy, L. J., Ramalingam, R. J., & Al-Lohedan, H. A. Green synthesis of NiO nanoparticles using Aegle marmelos leaf extract for the evaluation of in-vitro cytotoxicity, antibacterial and photocatalytic properties. *Journal of Photochemistry and Photobiology B: Biology*, **2018,** 180, 39-50.
78. Zewde, Dagme, & Belete Geremew, B. Removal of Congo red using Vernonia amygdalina leaf powder: optimization, isotherms, kinetics, and thermodynamics studies. *Environmental Pollutants and Bioavailability*, **2022,** 34.1, 88-101.
79. Widyaningtyas, A. L., Yulizar, Y., & Bagus Apriandanu, D. O. Ag_2O nanoparticles fabrication by Vernonia amygdalina Del. leaf extract: synthesis, characterization, and its photocatalytic activities. In *IOP Conference Series: Materials Science and Engineering*, IOP Publishing.**2019,** 509: 012022.
80. David, S. A., Doss, A., Pole, R. P. P., Rani, T. P. K. P., Reshmi, R. P. L., & Rajalakshmi, R. Synthesis and characterization of Cobalt Oxide nanoparticles using Momordica charantia and its photocatalytic activity. *International Journal of Nano Dimension* **2022**, 13(3), 335-343.
81. Ajeel, K. I., & Kareem, Q. S. Synthesis and characteristics of polyaniline (PANI) filled by graphene (PANI/GR) nano-films. In *Journal of Physics: Conference Series* IOP Publishing, **2019**, 34, 1742-1768
82. Chen, X., Chen, Y., Luo, X., Guo, H., Wang, N., Su, D. ... & Cui, L. Polyaniline engineering defect-induced nitrogen doped carbon-supported Co_3O_4 hybrid composite as a high-efficiency electrocatalyst for oxygen evolution reaction. *Applied Surface Science* **2020**, 526 146626.

83. X. Lu, Y. Ye, Y. Xie, Y. Song, S. Chen, P. Li, L.Chen, L. Wang, . Copper Coralloid Granule/ Polyaniline/ Reduced Graphene Oxide Nanocomposites for Nonenzymatic Glucose Detection. *Anaytical Methods* ,**2014** ,6, 4643−4651
84. Sawarkar, M., Pande, S. A., & Agrawal, P. S. Synthesis and characterization of polyaniline doped metal oxide nanocomposites. *International Research Journal of Engineering and Technology.* **2015**, 2 (9), 2427-2432
85. Suryyia Manzoor 1 , Ghazala Yasmin 1 , Nadeem Raza 2 , Javier Fernandez 3 , Rashida Atiq 4 , Sobia Chohan 4 , Ayesha Iqbal 1 , Shamaila Manzoor 5,*, Barizah Malik 6 , Franz Winter 7 and Mudassar Azam 7,8,*Pudukudy, M.; Yaakob, Z. Sol-gel synthesis, characterisation, and photocatalytic activity of porous spinel Co_3O_4 nanosheets. Chem. Pap. **2014**, 68, 1087–1096
86. Sohrabnezhad S, Pourahmed A, Radaee E; Photocstalytic degradation of basic blue 9 by CoS nanoparticles supported on AIMCM-41 material as a catalyst. *Journal of hazardous materials,* **2009**,170 (1), 158-165

APPENDICES

Appendix 1 different samples prepared and used in laboratory

a) $(NH_4)_2S_2O_8$

b) Aniline

c) Hydrochloric Acid

d) VA extracts

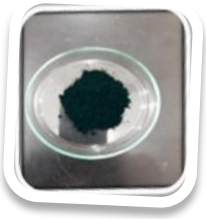

e) PANI

f) Co_3O_4

g) Co_3O_4/PANI

Appendix 2: effect of catalyst dose

Degradation of Methylene blue with volume of the sample 25 ml, A0 0.972, and dye concentration 10ppm with different catalyst dose of Co_3O_4 NPs

R.no	Catalyst Dosage	A0	At	% of degradation
1	0.02	0.972	0.357	63.27
2	0.04	0.972	0.251	74.17
3	0.06	0.972	0.114	88.27
4	0.08	0.972	0.117	87.96
5	0.1	0.972	0.138	85.80

Degradation of Congo red with volume of the sample 25 ml, A0 0.641, and dye concentration 15ppm with different catalyst dose of Co_3O_4 NPs

R. no	Catalyst dosage(gm.)	A0	At	% of degradation
1	0.01	0.641	0.235	63.33
2	0.03	0.641	0.181	71.76
3	0.06	0.641	0.115	85.05
4	0.09	0.641	0.075	88.29
5	0.12	0.641	0.081	87.36
s6	0.15	0.641	0.087	86.42

Degradation of Methylene blue with volume of the sample 25 ml, A0 0.972, and dye concentration 10ppm with different catalyst dose of Co_3O_4/PANI NCs

R. no	Catalyst Dosage	A0	At	% of degradation
1	0.02	0.972	0.276	71.60494
2	0.04	0.972	0.123	87.34568
3	0.06	0.972	0.089	90.84362
4	0.08	0.972	0.099	90.12346
5	0.1	0.972	0.099	89.81481

Degradation of Congo red with volume of the sample 25 ml, A0 0.641, and dye concentration 15ppm with different catalyst dose of Co_3O_4/PANI NCs

R. no	Catalyst dosage(gm.)	A0	At	% of degradation
1	0.01	0.641	0.185	71.13885
2	0.03	0.641	0.135	78.93916
3	0.06	0.641	0.080	87.5195
4	0.09	0.641	0.044	93.13573
5	0.12	0.641	0.051	92.04368
6	0.15	0.641	0.054	91.57566

Appendix 3: Effect of initial concentration

Degradation of Methylene blue with catalyst dose 0.06gm/25ml of Co_3O_4 NPs, with different dye concentration.

Rol.no	Concentration(ppm)	A0	At	% of degradation
1	1	0.145	0.0198	86.31
2	5	0.466	0.06	87.23
3	10	0.972	0.114	88.27
4	15	1.351	0.368	72.76
5	20	1.76	0.528	70

Degradation of Congo red with catalyst dose 0.09gm/25ml of Co_3O_4 NPs, and with different dye concentration.

R.no	Concentration (ppm)	A0	At	% of degradation
1	1	0.087	0.01	88.58
2	5	0.246	0.026	89.43
3	10	0.437	0.044	89.99
4	15	0.641	0.0583	90.90
5	20	0.923	0.221	76.05
6	25	1.185	0.325	72.57

Degradation of Methylene blue with volume of the sample 25 ml, catalytic dose 0.06gm of NCs A0 0.972, and with different dye concentration of MB.

Rol.no	Concentration(ppm)	A0	At	% of degradation
1	1	0.145	0.017	88.39
2	5	0.466	0.049	89.53
3	10	0.972	0.085	91.25
4	15	1.351	0.342	74.68
5	20	1.76	0.485	72.44

Degradation of Congo red with volume of the sample 25 ml, catalytic dose 0.09gm of NCs, and with different dye concentration of CR

R.no	Concentration (ppm)	A0	At	% of degradation
1	1	0.087	0.009	90.29
2	5	0.246	0.022	91.26
3	10	0.437	0.034	92.33
4	15	0.641	0.041	93.98
5	20	0.923	0.194	78.98
6	25	1.185	0.308	74

.

Appendix 4: Effect of PH

Degradation of Methylene blue with catalyst dose 0.06gm of Co_3O_4 NPs, volume of 25 ml, A0 0.972, and dye concentration of 10ppm.

Rol.no	PH	A0	At	% of degradation
1	4	0.972	0.239	75.41
2	6	0.972	0.199	79.52
3	8	0.972	0.157	83.84
4	10	0.972	0.101	89.60
5	12	0.972	0.177	81.79
6	14	0.972	0.205	78.90

Degradation of Congo red with catalyst dose 0.09gm of Co_3O_4 NPs, volume of 25 ml, A0 0.641, and dye concentration at15ppm.

R.no	PH	A0	At	% of degradation
1	4	0.641	0.139	78.31513
2	6	0.641	0.124	80.65523
3	8	0.641	0.059	90.79563
4	10	0.641	0.089	86.11544
5	12	0.641	0.109	82.99532
6	14	0.641	0.128	80.0312

Degradation of Methylene blue with catalyst dose 0.06gm of Co_3O_4 NCs, volume of 25 ml, A0 0.972, and dye concentration of 10ppm.

Rol.no	PH	A0	At	% of degradation
1	4	0.972	0.182	81.27572
2	6	0.972	0.166	82.92181
3	8	0.972	0.129	86.7284
4	10	0.972	0.081	91.66667
5	12	0.972	0.144	85.18519
6	14	0.972	0.149	84.67078

Degradation of Congo red with catalyst dose 0.09gm of Co_3O_4 NCs, volume of 25 ml, A0 0.641, and dye concentration of 15ppm.

R.no	PH	A0	At	% of degradation
1	4	0.641	0.099	84.55538
2	6	0.641	0.083	87.05148
3	8	0.641	0.0404	93.69735
4	10	0.641	0.069	89.23557
5	12	0.641	0.075	88.29953
6	14	0.641	0.092	85.64743

Appendix 5: Effect of exposure time

Degradation of Methylene blue with catalyst dose 0.06gm of Co_3O_4 NPs, volume of 25 ml, A0 0.972, pH 10 and dye concentration of 10ppm.

Rol.no	exposure time	A_0	At	% of degradation
1	15min	0.972	0.350	63.99
2	30 min	0.972	0.321	66.97
3	45 min	0.972	0.270	72.22
4	60 min	0.972	0.231	76.23
5	75 min	0.972	0.181	81.37
6	90 min	0.972	0.157	83.84
7	105 min	0.972	0.119	87.75
8	120 min	0.972	0.152	84.36
9	135 min	0.972	0.152	84.36

Degradation of Congo red with catalyst dose 0.09gm of Co_3O_4 NPs, volume of 25 ml, A0 0.641, PH 8 and dye concentration of 15ppm.

Rol.no	Exposure time	A_0	At	% of degradation
1	15min	0.641	0.226	64.74259
2	30 min	0.641	0.193	69.8908
3	45 min	0.641	0.146	77.22309
4	60 min	0.641	0.111	82.68331
5	75 min	0.641	0.08	87.5195
6	90 min	0.641	0.062	90.32761
7	105 min	0.641	0.071	88.92356
8	120 min	0.641	0.071	88.92356
9	135 min	0.641	0.071	88.92356

Degradation of Methylene blue with catalyst dose 0.06gm of Co_3O_4/PANI NPs, volume of 25 ml, A0 0.972, PH 10 and dye concentration of 10ppm.

Rol.no	exposure time	A0	At	% of degradation
1	15min	0.972	0.303	68.8271
2	30 min	0.972	0.249	74.38272
3	45 min	0.972	0.223	77.05761
4	60 min	0.972	0.182	81.27572
5	75 min	0.972	0.141	85.49383
6	90 min	0.972	0.131	86.52263
7	105 min	0.972	0.0861	91.14198
8	120 min	0.972	0.0894	90.80247
9	135 min	0.972	0.0896	90.78189

Degradation of Congo red with catalyst dose 0.09gm of Co_3O_4 NCs, volume of 25 ml, A0 0.641, PH 8 and dye concentration of 15ppm.

Rol.no	exposure time	A0	At	% of degradation
1	15min	0.641	0.206	67.86271
2	30 min	0.641	0.159	75.19501
3	45 min	0.641	0.112	82.5273
4	60 min	0.641	0.082	87.20749
5	75 min	0.641	0.054	91.57566
6	90 min	0.641	0.035	94.53978
7	105 min	0.641	0.046	92.82371
8	120 min	0.641	0.046	92.82371
9	135 min	0.641	0.046	92.82371

Appendix 6: Calibration curve data for MB and CR

R.no	Dyes	**Concentration(ppm)**	**Absorbance**
1	Methylene blue	1	0.145
2		5	0.466
3		10	0.972
4		15	1.351
5		20	1.760
7	Congo red	1	0.087
8		5	0.246
9		10	0.437
10		15	0.641
11		20	0.923
12		25	1.185

Appendix 7: catalyst reusability

Reusability of Co_3O_4 NPs for the degradation of methylene blue and Congo red at optimum condition

Number of cycle	**Dyes**	**A_t**	% of degradation
1st	Methylene blue	0.120917	87.56
	Congo red	0.066344	89.65
2nd	Methylene blue	0.126652	86.97
	Congo red	0.072369	88.71
3rd	Methylene blue	0.13851	85.75
	Congo red	0.081343	87.31
4th	Methylene blue	0.146869	84.89
	Congo red	0.088394	86.21

Reusability of Co_3O_4/PANI nanocomposites for the degradation of methylene blue and Congo red at optimum condition

Number of cycle	**Dyes**	**A_t**	**% of degradation**
1st	Methylene blue	0.096617	90.06
	Congo red	0.047242	92.63
2nd	Methylene blue	0.107309	88.96
	Congo red	0.057626	91.01
3rd	Methylene blue	0.125194	87.12
	Congo red	0.066087	89.69
4th	Methylene blue	0.130442	86.58
	Congo red	0.074292	88.41